Published online 24 July 2023

Nucleic Acids Research, 2023, Vol. 51, No. 17 ***9101–9121***
https://doi.org/10.1093/nar/gkad612

ISW1a modulates cohesin distribution in centromeric and pericentromeric regions

Ireneusz Litwin [1,*], Małgorzata Nowicka[2], Katarzyna Markowska[1], Ewa Maciaszczyk-Dziubińska[2], Paulina Tomaszewska[2,3], Robert Wysocki [2] and Karol Kramarz[1]

[1]Academic Excellence Hub - Research Centre for DNA Repair and Replication, Faculty of Biological Sciences, University of Wroclaw, 50-328 Wroclaw, Poland, [2]Department of Genetics and Cell Physiology, Faculty of Biological Sciences, University of Wroclaw, 50-328 Wroclaw, Poland and [3]Department of Genetics and Genome Biology, University of Leicester, Leicester LE1 7RH, UK

Received October 03, 2022; Revised June 28, 2023; Editorial Decision June 29, 2023; Accepted July 11, 2023

ABSTRACT

Cohesin is a highly conserved, multiprotein complex whose canonical function is to hold sister chromatids together to ensure accurate chromosome segregation. Cohesin association with chromatin relies on the Scc2-Scc4 cohesin loading complex that enables cohesin ring opening and topological entrapment of sister DNAs. To better understand how sister chromatid cohesion is regulated, we performed a proteomic screen in budding yeast that identified the Isw1 chromatin remodeler as a cohesin binding partner. In addition, we found that Isw1 also interacts with Scc2-Scc4. Lack of Isw1 protein, the Ioc3 subunit of ISW1a or Isw1 chromatin remodeling activity resulted in increased accumulation of cohesin at centromeres and pericentromeres, suggesting that ISW1a may promote efficient translocation of cohesin from the centromeric site of loading to neighboring regions. Consistent with the role of ISW1a in the chromatin organization of centromeric regions, Isw1 was found to be recruited to centromeres. In its absence we observed changes in the nucleosomal landscape at centromeres and pericentromeres. Finally, we discovered that upon loss of RSC functionality, ISW1a activity leads to reduced cohesin binding and cohesion defect. Taken together, our results support the notion of a key role of chromatin remodelers in the regulation of cohesin distribution on chromosomes.

GRAPHICAL ABSTRACT

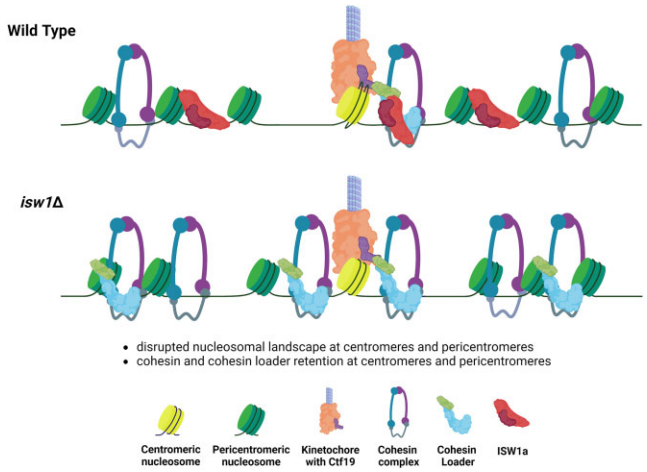

INTRODUCTION

Faithfull division of genetic material is of fundamental importance for all organisms since errors in chromosome segregation are one of the main factors that drive genomic instability. To ensure equal separation of DNA, sister chromatids are held together from S phase to metaphase–anaphase transition by a multiprotein complex called cohesin. This makes it possible to establish chromosome biorientation, counteracts the pulling force of mitotic spindle microtubules, preventing premature sister chromatid separation, and ensures precise segregation of sister DNAs into daughter cells (1–3). The core cohesin complex is composed of two rod-shaped ATPases, Smc1 and Smc3, that are bridged by a kleisin subunit, Scc1. The resulting assembly is a large tripartite ring, which topologically entraps sister chromatids (4,5). Scc1 also associates with two essential HEAT proteins, Scc3 and Pds5, and with nonessential, loosely bound Wpl1, which also interacts with Pds5 and

*To whom correspondence should be addressed. Tel: +48 71 375 4126; Fax: +48 71 375 4118; Email: ireneusz.litwin@uwr.edu.pl

possibly with Smc3 (6–10). In budding yeast, most cohesins start to associate with chromatin in late G1/early S phase, when the kleisin subunit becomes resynthesized after cleavage by Esp1 separase in previous anaphase (1,11,12). Cohesin loading is mediated by a separate complex that consists of Scc2 HEAT protein (NIPBL in humans) that together with Scc4 (MAU2 in humans) creates a hook-shaped structure that is crucial for cohesin association with chromatin (12–14). Recent studies suggest that entrapment of chromatids inside the cohesin ring involves direct interaction between the cohesin loader, cohesin and DNA, followed by Scc2-driven ATP hydrolysis, which enables opening of the ring (12,14–17). Stable entrapment of sister chromatids within cohesin takes place during DNA replication and depends on acetylation of Lys112 and Lys113, located on the Smc3 head, by the PCNA-binding partner Eco1 acetyltransferase (14,18–20). Next, Pds5 and Scc3 maintain cohesion of sister chromatids until the onset of anaphase, when separase cleaves Scc1, creating an exit gate for the DNA (21–23).

In budding yeast, two populations of chromatin-bound cohesin can be distinguished, one loaded on chromosome arms and one loaded at centromeres (CENs). Cohesin that associates with chromosome arms is loaded by the Scc2-Scc4 complex preferentially at certain gene promoters, especially tRNA genes, ribosomal protein genes and telomeres (12,24,25). After association with the chromatin, these cohesin rings are most likely pushed away from loading sites by transcription machinery usually between genes transcribed convergently (25,26). The second population of cohesin is loaded by Scc2-Scc4 at CENs by a mechanism dependent mainly on the kinetochore. In budding yeast, CENs are defined, ∼120 bp long DNA fragments wrapped around a single nucleosome (CEN nucleosome) that contains the centromere-specific H3 histone variant Cse4 (CENP-A in humans). It recruits a multiprotein kinetochore complex that binds the spindle microtubule polymer to direct chromosome alignment and segregation (27). CTF19 (CCAN in humans) is an inner kinetochore subcomplex that recognizes Cse4 and supports outer kinetochore assembly (28). Interestingly, recent reports suggest that it is also crucial for centromeric cohesion. It was demonstrated that, already in G1 phase of the cell cycle, Ctf19 (CENP-P in humans), a subunit of the CTF19 complex, becomes phosphorylated by Dbf4-dependent kinase (DDK), and recruits cohesin loader through interaction with Scc4, ensuring extensive and targeted cohesin association with CENs (29). Following loading, centromeric cohesin relocates to nearby regions called pericentromeres (periCENs) that span on average several kilobases around CENs (12,30–33).

Chromatin remodelers play an important role in sister chromatid cohesion (SCC). In budding yeast, the RSC chromatin remodeler complex directly interacts with cohesin loader and cohesin (34,35). Recent evidence suggests that RSC recruits cohesin loader to chromatin independently of chromatin remodeling activity; however, optimal cohesin association with chromatin requires the Sth1 ATPase subunit (34). Consequently, disruption of RSC leads to decreased levels of chromatin-bound cohesin and precocious sister chromatid separation (24,34,36,37). Moreover, other yeast chromatin remodelers were also implicated in SCC. Our previous research has shown that Irc5 translocase contributes to Scc2 association with chromatin and cohesin. Furthermore, like RSC, Irc5 interacts with cohesin. Disruption of *IRC5* or its ATPase activity led to decreased levels of chromatin-bound cohesin, resulting in mild premature sister chromatid separation (38). Also Chd1 seems to play a role in SCC as its disruption resulted in reduced cohesin association with chromatin and a cohesion defect along chromosome arms (39). Lastly, recent data suggest a role of Isw1 in cohesion specifically at *HMR* loci (40).

Isw1 belongs to the Snf2 family of chromatin remodelers that alter the interaction between DNA and histones using energy derived from ATP hydrolysis (41,42). It is a major yeast protein that regulates nucleosome spacing *in vivo*. Average nucleosome spacing decreases from ∼166 bp in wild type cells to ∼159 bp in the *isw1*Δ mutant. Nucleosomes also show weaker phasing in cells lacking Isw1 (43–45). Importantly, despite the disruption of the chromatin structure, only subtle changes in expression of a limited number of genes were observed in *isw1*Δ cells (43–49). However, Isw1 supports proper chromatin organization during transcription and contributes to dissolution of dinucleosomes, limiting intragenic, cryptic transcription (44,50). Interestingly, Isw1 is an ATPase subunit of at least two different complexes, ISW1a and ISW1b, that contain either Ioc3 or Ioc2/Ioc4 proteins, respectively (46). Genome-wide studies revealed that Isw1 occupies most genes and is present at all genic nucleosome positions. It also associates with −1 and −2 nucleosomes. On the other hand, Ioc3 binds to −2 and + 1 nucleosomes while Ioc4 occupies nucleosomes + 2, +3 and + 4. These data suggest that Ioc subunits may direct Isw1 to specific genomic locations (50–52).

In order to better understand how SCC is regulated, we pulled down Scc1 and performed mass spectrometry (MS) analysis of copurified proteins. We found that the Isw1 chromatin remodeler is a binding partner of cohesin and the cohesin loader. We observed that deletion of *ISW1* or *IOC3* led to CTF19-dependent accumulation of cohesin at CENs and periCENs, suggesting that the ISW1a complex supports translocation of cohesin from CENs to periCENs. We also provide evidence that Isw1 and RSC balance each other to modulate centromeric cohesin association.

MATERIALS AND METHODS

Yeast strains and growing conditions

The *Saccharomyces cerevisiae* strains used in this study are listed in Supplementary Table S1. Yeast cells were grown in complete YPD medium at 30°C. Gene deletion or tagging was performed using a PCR-based method (53–56). Multiple gene mutants were obtained by genetic crossing of relevant haploids followed by tetrad dissection. To assess the sensitivity of relevant strains to thiabendazole (TBZ), mid-log cultures were 10-fold serially diluted and spotted on solid media containing indicated concentrations of the drug. For each strain several clones were tested. Representative images are shown. Cell doubling time was calculated as described previously (57).

Scc1-TAP purification and MS analysis

Approximately 10^{11} of logarithmically growing untagged or Scc1-TAP cells were harvested by centrifugation, extensively washed with water and YEB buffer (100 mM HEPES–KOH pH 7.9, 200 mM KCl, 5 mM EDTA, 5 mM EGTA, 2 mM DDT, protease inhibitors [Sigma-Aldrich, P8215], 1 mM PMSF) and then snap-frozen in liquid nitrogen. Cells were lysed by grinding in the presence of dry ice. Lysed powders were reconstituted in YEB buffer on ice followed by 15 min centrifugation at 4000 rpm. Next, supernatants were transferred to new tubes and centrifuged for 30 min at 15 000 rpm. Resulting protein extracts were incubated with IgG Sepharose beads (GE Healthcare, 17-0969–01) for 2 h at 4°C with rotation and then centrifuged for 1 min at 1500 rpm. Next, beads were washed several times with IPP buffer (10 mM Tris pH 7.9, 100 mM NaCl, 0.1% Triton X) and then with TEV buffer (50 mM Tris pH 7.9, 0.2 mM EDTA, 100 mM NaCl, 0.1% Triton X, 1 mM DDT). To release Scc1, IgG Sepharose beads were incubated overnight at 4°C in TEV buffer containing 400 U of TEV protease. The next day, beads were separated from the buffer and the released proteins were precipitated with the methanol-chloroform procedure. Protein pellets were resuspended in 100 mM ammonium bicarbonate and subjected to the standard procedure of trypsin digestion, including reduction with 0.5 M TCEP for 1 h at 60°C, blocking with 200 mM MMTS for 10 min at room temperature (RT) followed by overnight digestion with 10 μl of 0.1 μg/μl trypsin. The resulting peptide mixtures were applied in equal volumes of 20 μl to an RP-18 pre-column (Waters, Milford, MA) using water containing 0.1% FA as a mobile phase and then transferred to a nano-HPLC RP-18 column (internal diameter 75 μM, Waters, Milford MA) using an ACN gradient (0–35% ACN in 160 min) in the presence of 0.1% FA at a flow rate of 250 μl/min. The column outlet was coupled directly to the ion source of the Q Exactive mass spectrometer (Thermo Electron Corp., San Jose, CA) working in the regime of data-dependent MS to MS/MS switch. A blank run ensuring absence of cross-contamination from previous samples preceded each analysis. MS/MS data were preprocessed with Mascot Distiller software (v. 2.6, MatrixScience, London, UK) and a search was performed with the Mascot Search Engine (MatrixScience, London, UK, Mascot Server 2.6) against the SGD database. To reduce mass errors, the peptide and fragment mass tolerance settings were established separately for individual LC-MS/MS runs after a measured mass recalibration. The rest of the search parameters were as follows: enzyme, trypsin; missed cleavages, 1; fixed modifications, methylthio (C); variable modifications, oxidation (M); instrument, HCD. The Decoy Mascot functionality was used for keeping FDR for peptide identifications below 1%. To analyze raw MS data, we removed proteins that were present in a control preparation from an untagged strain. To eliminate other nonspecific hits, we used the Crapome database (https://reprint-apms.org/?q = reprint-home) as well as common background contaminant lists reported previously (58,59). Finally, we verified the localization of remaining proteins using SGD (https://www.yeastgenome.org/) and eliminated proteins solely localized in the cytoplasm.

Proximity ligation assay

For every sample, 10^7 of logarithmically growing cells were fixed with 4% formaldehyde for 15 min at RT and then washed twice with ST buffer (1 M sorbitol, 20 mM Tris pH 7.5). To digest cell wall, cells were incubated in Zymolyase buffer (10 mg/ml Zymolyase [BioShop, ZYM001.1], 1 M sorbitol, 20 mM Tris pH 7.5, 0.5% 2-mercaptoethanol) for 60 min at 30°C. The resulting spheroplasts were washed with ST buffer and permeabilized with methanol for 5 min at RT. Next, cells were incubated for 60 min at 37°C with Duolink blocking solution (Sigma-Aldrich, DUO82007), followed by 5 min centrifugation at 1000 rpm. Then, cells were resuspended in 100 μl of Duolink antibody diluent (Sigma-Aldrich, DUO82008) containing appropriate antibody (Sigma-Aldrich anti-HA, H6908; Roche anti-HA, 11583816001; Bio-Rad anti-Pk, MCA1360G; Roche anti-cMyc, 11667149001; Sigma-Aldrich anti-FLAG, F1804; Abcam anti-Rad53, ab104232; anti-Pma1, Dr. Ramon Serrano) and incubated overnight at 4°C. The next day, cells were centrifuged for 5 min at 1000 rpm, washed twice with Duolink Wash Buffer (Sigma-Aldrich, DUO82047) and resuspended in 100 μl of Duolink antibody diluent containing Duolink Probe Anti-Mouse Plus (Sigma-Aldrich, DUO92001) and Duolink Probe Anti-Rabbit Minus (Sigma-Aldrich, DUO92005) followed by 60 min incubation at 37°C. The proximity ligation reaction was performed using Duolink flowPLA Detection Kit-Green (Sigma-Aldrich, DUO94002) according to the manufacturer's guideline with some minor modifications. After incubation with anti-Mouse and anti-Rabbit probes, cells were centrifuged, washed twice with Duolink Wash Buffer and resuspended in 50 μl of ligation buffer containing 1.25 μl of ligase for 30 min at 37°C. Next, cells were washed twice with Duolink Wash Buffer and incubated for 100 min at 37°C in 50 μl of amplification buffer including 0.62 μl of DNA polymerase. After completion of incubation, cells were centrifuged once more, washed twice with Duolink Wash Buffer and incubated in 50 μl of Detection Solution (Sigma-Aldrich, DUO84002) for 30 min at 37°C in the dark. Finally, cells were washed with Duolink Wash Buffer, diluted and analyzed with a Millipore Guava EasyCyte flow cytometer. Each proximity ligation assay (PLA) analysis was performed at least 3 times. Relative fluorescence intensity values for indicated strain and antibody combinations are presented in Supplementary Data Set S2.

Coimmunoprecipitation

Native extracts for immunoprecipitation were prepared from approximately 5×10^8 cells. Cell pellets were resuspended in 600 μl of ice-cold IP buffer (50 mM HEPES–KOH pH 7.5, 100 mM KCl, 2.5 mM $MgCl_2$, 10% glycerol, 0.25% Triton X, protease inhibitors [Sigma-Aldrich, P8215], 1 mM PMSF) and lysed in a bead beater at 4°C. Then, whole cell extracts were centrifuged for 15 min at 15000 rpm and 500 μl of cleared lysates were transferred to new tubes. To digest nucleic acids, lysates were incubated with 500 U of Benzonase (Sigma-Aldrich, E8263) and 100 U of RNase (Thermo Fisher, EN0601) for 1 h at 4°C on a rotator wheel. To capture HA or PK tagged proteins, lysates

were incubated for 2 h at 4°C with Protein G Dynabeads (Thermo Fisher, 10003D) pre-coated with either anti-HA (Sigma-Aldrich, H6908) or anti-Pk antibodies (Bio-Rad, MCA1360G). Upon completion of incubation, the beads were washed 4 times with IP buffer followed by protein elution with Laemmli buffer (2% SDS, 20% glycerol, 120 mM Tris pH 6.8, 4% 2-mercaptoethanol, 0.01% bromophenol blue). Proteins were resolved on Mini Protean TGX gels (Bio-Rad, 4561096). 1% of whole cell extract volume used for immunoprecipitation was analyzed as input. To assess pull-down efficiency, one tenth of the eluted fraction was analyzed using antibody directed to precipitated protein. The rest of the eluate was used to detect the potential binding partner. Each coimmunoprecipitation (CoIP) analysis was performed 3 times with similar results.

Pull-down assay in *Escherichia coli*

SCC1-cMyc as well as the N-terminal (1–120 aa), middle (121–459 aa) and C-terminal (460–567 aa) truncations of *SCC1*, tagged with cMyc, were cloned into the pACYCDuet-1 vector. Isw1 was cloned into the pET Flag TEV LIC vector (Supplementary Table S2). Proteins were expressed in BL21 *E. coli* cells grown in auto-induction medium (0.5% yeast extract, 2% tryptone, 0.5% NaCl, 0.6% glycerol, 0.05% glucose, 0.2% lactose, 25 mM phosphate buffer, pH 7.2) supplemented with antibiotics (30 μg/ml kanamycin, 35 μg/ml chloramphenicol) for 20 h at 37°C. To lyse cells, *E. coli* pellets were resuspended in Lysis mix (50 mM sodium phosphate, 300 mM NaCl, 2.5 mM magnesium acetate, 0.5% *N*-decyl-B-D-maltoside, 2 mg/ml lysozyme, 0.2 mg/ml DNase, 0.2 mg/ml RNase) and rotated at RT for 15 min. Next, lauroylsarcosine was added (1% final) followed by 15 min centrifugation at 12 000 rpm. Resulting lysates were supplemented with NP40 (0.02% final) and incubated with prewashed cMyc nanobodies (ChromoTek Myc-Trap Agarose) overnight, at 4°C on a rotator wheel. The next day, beads were washed 3 times with DB buffer (50 mM sodium phosphate, 300 mM NaCl, 2.5 mM magnesium acetate, 0.5% *N*-decyl-B-D-maltoside, 0.05% NP40) followed by protein elution with Laemmli buffer. Proteins were resolved on Mini Protean TGX gels (Bio-Rad, 4561096) and analyzed using anti-cMyc (Roche, 11667149001) and anti-FLAG (Sigma-Aldrich, F1804) antibodies.

Cell cycle analysis

To arrest yeast in G1 phase, cells were cultured in YPD in the presence of 5 μM α-factor for 2 h. G2/M block was achieved by incubating cells in YPD containing 15 μg/ml nocodazole (Sigma-Aldrich, M1404) for 2 h. G1 and G2/M arrests were confirmed by microscopic observations and FACS analysis. To measure DNA content, cell samples were collected and fixed with 70% ethanol. Next, cells were digested with 0.25 mg/ml RNase for 2 h at 50°C and with 5 mg/ml pepsin for 1 h at 37°C. Then, cells were sonicated and stained with 0.5 μM Sytox Green (Thermo Fisher, S7020) for 30 min at RT in the dark. FACS analysis was performed using a Millipore Guava EasyCyte flow cytometer. To determine the fraction of post-mitotic cells, aliquots were fixed, stained as for flow cytometry, and then observed with an Axio Imager M1 epifluorescence microscope (Carl Zeiss, Germany) equipped with a 100x immersion oil objective (Plan-Neofluar 1006/1.30), the GFP filter set and differential interference contrast (DIC) to score the percentage of binucleate large-budded cells.

Cohesion assay

To assess premature sister chromatid cohesion levels, cells carrying GFP-marked CEN IV +2.4 kb, *URA3* or *LYS4* loci were arrested in either G1 or G2/M. Next, cells were fixed with 4% formaldehyde and resuspended in SK buffer (1 M sorbitol, 0.05 M K_2PO_4). Cells were observed with the Axio Imager M1 epifluorescence microscope (Carl Zeiss, Germany) equipped with a 100x immersion oil objective (Plan-Neofluar 1006/1.30), the GFP filter set and differential interference contrast (DIC). Z-stacked images were collected using an AxioCam MRc digital color camera and processed with AxioVision 4.5 software. The cohesion assay was performed at least twice using two clones of each strain. A minimum of 200 cells were scored for each clone.

RNA extraction, reverse transcription and quantitative PCR

To measure *SCC1* and *SCC2* mRNA level, total mRNA was isolated using an RNeasy Mini Kit (Qiagen). Reverse transcription was performed with 1.5 μg of purified DNase treated RNA using a High-Capacity cDNA Reverse Transcription Kit (Applied Biosystems) according to the manufacturer's instructions. Quantitative PCR (qPCR) reactions were carried out using the CFX Connect Real-Time PCR System (Bio-Rad) with SsoAdvanced Universal SYBR Green Supermix (Bio-Rad, 1725272) and the *SCC1* and *SCC2* primer set (Supplementary Table S3) in a total volume of 15 μl. All results were standardized using the reference gene *IPP1*, with the IPP1 primer set (Supplementary Table S3). The following conditions of amplifications were applied: 30 s at 98°C; 35 cycles of 15 s at 95°C and 20 s at 57°C. mRNA measurements were repeated 3 times and every sample was used for qPCR twice.

Chromatin immunoprecipitation

For Scc1-9Pk chromatin immunoprecipitation (ChIP), $\sim 5 \times 10^8$ cells were fixed with 1% formaldehyde for 15 min at RT and then rocked for 5 min with 150 mM glycine. Next, cells were collected by centrifugation, washed once with TBS buffer and resuspended in 600 μl of FA-lysis buffer (50 mM HEPES-KOH pH 7.5, 140 mM NaCl, 1 mM EDTA, 0.1% sodium deoxycholate, 1% Triton X, protease inhibitors [Sigma-Aldrich, P8215], 1 mM PMSF). Cells were lysed by 2 rounds of bead-beating at 4000 rpm for 30 s. Next, whole cell extracts were transferred to new tubes and sonicated to yield an average DNA size of 500 bp followed by 30 min centrifugation at 15 000 rpm. Cleared lysates were moved to new tubes and 1% of the lysates were kept as an input sample. For the IP reaction, 5 μl of anti-Pk antibodies (Bio-Rad, MCA1360G) were added to the lysates and incubated overnight at 4°C on a rotator wheel.

The next day, DNA-protein complexes were captured with Protein G Dynabeads (Thermo Fisher, 10003D) and sequentially washed with FA-lysis buffer, FA-500 buffer (50 mM HEPES–KOH pH 7.5, 500 mM NaCl, 1% Triton X-100, 0.1% sodium deoxycholate, 1 mM EDTA), LiCl wash buffer (10 mM Tris–HCl pH 8.0, 250 mM LiCl, 0.5% NP-40, 0.5% sodium deoxycholate, 1 mM EDTA) and TE (10 mM Tris–HCl pH 7.5, 1 mM EDTA) on a rotator for 5 min each time. Beads and input samples were then resuspended in elution buffer (50 mM Tris–HCl pH 7.5, 1% SDS, 10 mM EDTA) and incubated at 65°C for 2 h on a thermal shaker. Finally, DNA was recovered using a Monarch PCR & DNA Cleanup Kit (New England BioLabs, T1030L). qPCR reactions were performed using both IP and input samples as templates, SsoAdvanced Universal SYBR Green Supermix (Bio-Rad, 1725272) and the CFX Connect Real-Time PCR System (Bio-Rad) in a total volume of 15 μl. Primers used for qPCR are listed in Supplementary Table S3. The following conditions of amplifications were applied: 30 s at 98°C; 35 cycles of 15 s at 95°C and 20 s at 57°C. The percentage (% input) value for each sample was calculated as follows: ΔCT [normalized ChIP] = CT [ChIP] − {CT [Input] − $\log_2$ (dilution factor)} and Input % = $100/^{2\Delta CT\ [\text{normalized ChIP}]}$. The fold enrichment value represents the % input value normalized to the *ACT1* reference gene. Each ChIP analysis was performed at least 3 times.

For Scc2-9Pk chromatin immunoprecipitation, ∼10^9 of cells were fixed with 1% formaldehyde for 30 min at RT and then incubated for 5 min with 150 mM glycine. Cells were then collected by centrifugation, washed once with TBS buffer and snap-frozen in liquid nitrogen. Next, cell pellets were resuspended in 600 μl of FA-lysis buffer (50 mM HEPES–KOH pH 7.5, 140 mM NaCl, 1 mM EDTA, 0.1% sodium deoxycholate, 1% Triton X, protease inhibitors [Sigma-Aldrich, P8215], 1 mM PMSF). Cells were lysed by 4 rounds of bead-beating at 6000 rpm for 30 s. Next, whole cell extracts were transferred to new tubes and sonicated to yield an average DNA size of 500 bp followed by 30 min centrifugation at 15 000 rpm. Cleared lysates were transferred to new tubes and 400 μl of fresh FA-lysis buffer was added. 1% of the lysates was kept as an input sample. For IP reaction, 10 μl of anti-Pk antibodies (Bio-Rad, MCA1360G) were added to the rest of the protein extract and incubated overnight at 4°C on a rotator wheel. Bead wash, protein elution, DNA purification, qPCR conditions and the % of input calculations were as described above. Scc2 ChIP experiments were performed 3 times.

For ChIP experiments using Isw1-12Pk and Sth1-12Pk, ∼10^9 of cells were fixed with 1% formaldehyde for 30 min at RT and then incubated for 5 min with 150 mM glycine. Lysis and sonication conditions were as for ChIP of Scc2. For IP reaction, lysate was divided in half. 10 μl of anti-Pk antibodies (Bio-Rad, MCA1360G) was added to one part, while the other part was supplemented with 10 μl of unrelated normal IgG and incubated overnight at 4°C on a rotator wheel. Bead wash, protein elution, DNA purification and qPCR conditions were as for ChIP of Scc1. Fold enrichment was calculated by dividing % input values for a specific Pk signal by the IgG control. Isw1-12Pk experiments were performed 3 times while the Sth1-12Pk ChIP experiment was performed twice.

Calibrated ChIP-seq

For calibrated ChIP-seq, ∼3×10^8 *S. cerevisiae* cells expressing Scc1-9Pk were mixed with ∼10^8 *Schizosaccharomyces pombe* cells expressing Rad21-6HA, fixed with 1% formaldehyde for 15 min at RT and then rocked for 5 min with 150 mM glycine. Next, cells were collected by centrifugation, washed once with TBS buffer and resuspended in 600 μl of FA-lysis buffer (50 mM HEPES–KOH pH 7.5, 140 mM NaCl, 1 mM EDTA, 0.1% sodium deoxycholate, 1% Triton X, protease inhibitors [Sigma-Aldrich, P8215], 1 mM PMSF). Cells were lysed by 4 rounds of bead-beating at 6500 rpm for 30 s. Next, whole cell extracts were transferred to new tubes and sonicated to yield an average DNA size of 500 bp followed by 30 min centrifugation at 15 000 rpm. Cleared lysates were moved to new tubes and 2% of the lysates were kept as an input sample. For the IP reaction, 7 μl of anti-Pk antibodies (Bio-Rad, MCA1360G) and 3 μl of anti-HA (Roche,11583816001) were added to the lysates and incubated overnight at 4°C on a rotator wheel. The next day, DNA-protein complexes were captured with Protein G Dynabeads (Thermo Fisher, 10003D) and sequentially washed as described for ChIP of Scc1. Beads and input samples were then resuspended in elution buffer (50 mM Tris–HCl pH 7.5, 1% SDS, 10 mM EDTA) and incubated at 65°C for 2 h on a thermal shaker. Next, beads were removed and the IP eluates and input samples were incubated at 65°C overnight. Next day, all samples were treated with RNase A (100 μg/ml) for 1 h at 37°C followed by 2 h incubation at 65°C in the presence of proteinase K (1 mg/ml). Finally, DNA was recovered using a Monarch PCR & DNA Cleanup Kit (New England BioLabs, T1030L). DNA libraries were constructed using the NGS DNA Library Prep Set (Novogene, PT004). Sequencing was performed using the Illumina Novaseq 6000 platform.

ChIP-seq data analysis

The adapter sequences and low-quality bases were trimmed off using Skewer (60). Filtered reads were mapped against the target genome (*S. cerevisiae* S288C assembly SacCer3) and against the spike-in genome (*S. pombe* assembly ASM294v2) using BWA (61). Unmapped reads, rDNA regions, mitochondrial DNA and duplicates were filtered out using Samtools (62). Peaks were called using MACS2 (63). In order to visualize mapped reads, bigWig files were created using deepTools (64). The ChIPs were normalized against the input with counts per million (CPM) method. Samtools was used to count reads mapped to SacCer3 and ASM294v2 only, and these values were used to calculate the occupancy ratio value as shown previously (65). Plots were created around the midpoint of CENs.

MNase-seq data analysis

Raw data used to obtain nucleosome maps for wild type and *isw1*Δ cells were retrieved from the GEO database with accession number GSE69400 (44,45). Cutadapt was used to remove adapter sequences from high-throughput sequencing reads (66). Filtered reads were mapped to the *S. cerevisiae* reference genome version SacCer3 using Bowtie2 with

sensitive parameters (67,68). Samtools fixmate was run on the sorted alignments to label paired-end reads correctly. Duplicated reads were marked with samtools markdup and removed (62). Resulting BAM files were then filtered for proper pairs with a mapping score > 30 using samtools view. Mononucleosomes were identified as paired-end reads with insert sizes between 100 and 200 bp (69,70) using samtools view (62) and used as the input for Danpos software (71). Nucleosome scores from each of the studied samples were normalized to the same distribution using quantile normalization. The Dpos function was used to analyze changes in the location, fuzziness and occupancy at canonical nucleosomes adjacent to centromeric nucleosomes. To obtain a sufficient smoothing effect, we used the window size of 100 bp and the step size of 10 bp. Genomic coordinates were downloaded from the UCSC Genome Browser (http://genome.ucsc.edu).

RESULTS

Identification of novel putative cohesin interactors by Scc1-TAP purification

In an effort to identify novel putative cohesin interactors, we constructed a yeast strain endogenously expressing TAP-tagged Scc1 (Scc1-TAP). Next, we performed a single-step TAP purification using an untagged strain (mock sample) or a strain expressing Scc1-TAP, followed by identification of co-purifying proteins by MS. After several curation steps we obtained a data set including 365 hits (Supplementary Data Set S1 Tables 1 and 2). To validate the capability of our approach to identify cohesin interactors, we looked for previously known, well-established Scc1 binding partners. We found that all cohesin subunits, including Smc1, Smc3, Scc3 and Pds5, were present in our data set (5,8,12,14,72). Furthermore, MS analysis of Scc1 was enriched in other cohesin interactors such as Cdc5 kinase and the RSC complex (34,36,73,74) (Table 1 and Supplementary Data Set S1 Table 2). On the other hand, we failed to recover some other cohesin binding partners such as Wpl1, Eco1, Spt16 and Irc5. Moreover, only a few peptides of proteins forming the cohesin loader were present in our data set (Supplementary Data Set S1 Table 2) (6,7,32,38,75–78). Together, this indicates that our protocol for single-step TAP purification of Scc1 allows stably associated cohesin interactors to be co-purified, but binding partners that turn over rapidly and/or bind cohesin at a specific cell-cycle stage may be underrepresented. Next, we performed Gene Ontology analysis of biological processes of proteins identified as putative cohesin interactors. We found that most of the proteins identified by MS were involved particularly in regulation of DNA transcription, mRNA processing, and chromatin remodeling, and could be grouped into a number of complexes (Supplementary Data Set S1 Tables 3 and 4). This is consistent with several previous reports pointing to the role of cohesin in regulation of gene expression in budding yeast (79–81). Interestingly, a recent MS analysis of the Scc2 interactome revealed a similar set of binding partners (82). These data support our MS results and suggest that, as for RSC, at least in some cases interaction between cohesin, the cohesin loader and a binding partner may occur at the same time (34, (83). Finally, we wondered whether yeast homologs of human cohesin interactors could be found in our data set. Interestingly, our MS results were enriched in Top2, the Mediator complex and splicing factors whose human counterparts are well characterized binding partners of human cohesin (Supplementary Data Set S1 Table 2) (84–86). This suggests that some of the identified interactions may be conserved and play a fundamental role in all eukaryotes. Intriguingly, our results revealed that several chromatin remodelers were enriched in our pull-downs, including RSC, Isw1 and Chd1. While the RSC complex is a well-established cohesin interactor, far less is known about the involvement of other chromatin remodelers in SCC. In this research, we set out to investigate the potential role of Isw1 in SCC.

Table 1. Results of proteomic analysis of Scc1-TAP associated proteins. Top 30 hits are shown. See Supplementary Data Set S1 for details

Protein	Accession	Score	Mass	Unique sequences	emPAI
SMC3	YJL074C	18118	141388	113	28.46
SMC1	YFL008W	13387	141469	100	18.37
SCC1	YDL003W	5810	63343	35	9.28
SCC3	YIL026C	2566	133432	35	2.04
ISW1	YBR245C	662	131434	18	0.79
ECM16	YMR128W	654	145324	16	0.59
MTR4	YJL050W	797	122530	15	0.68
UBR1	YGR184C	464	226673	15	0.32
STH1	YIL126W	288	156922	14	0.46
NOT3	YIL038C	516	94529	14	0.87
MBF1	YOR298C-A	703	16394	13	2.59
SPT5	YML010W	618	115718	13	0.61
HRP1	YOL123W	725	59705	12	1.33
NSP1	YJL041W	644	86464	12	0.80
RSC8	YFR037C	439	63451	11	1.08
PTK2	YJR059W	459	91711	11	0.66
CRP1	YHR146W	577	51177	10	1.28
ECM1	YAL059W	495	23877	10	4.75
YAP1	YML007W	475	72764	10	0.79
SEC13	YLR208W	447	33161	10	2.54
PAT1	YCR077C	424	88456	10	0.61
TOP2	YNL088W	421	164526	10	0.29
CHD1	YER164W	336	168413	10	0.29
RSC2	YLR357W	334	102466	10	0.51
UFD4	YKL010C	321	168795	10	0.29
SPB1	YCL054W	301	96701	10	0.55
DIM1	YPL266W	285	36066	10	2.20
DEF1	YKL054C	488	83923	9	0.50
PAP1	YKR002W	383	64879	9	0.80
DIS3	YOL021C	399	114325	8	0.34

Validation of Isw1 as a cohesin interacting protein

First, we decided to confirm the interaction between Isw1 and cohesin. To this end, we performed PLA. PLA is routinely used in mammalian cells to study protein-protein interactions and recently it has been successfully performed in yeast (Supplementary Figure S1) (87–91). To validate this method, we used an untagged strain as well as a strain with Scc1 and Scc3 cohesin subunits tagged with 6HA and 13cMyc, respectively, and performed PLA coupled to flow cytometry. We found that incubation of the untagged strain with anti-HA and anti-cMyc antibodies resulted in a basal fluorescent signal. Incubation of the Scc1-6HA Scc3-13cMyc strain with no primary antibodies or with either anti-HA or anti-cMyc antibody resulted in a similar level of autofluorescence. Only incubation of the tagged strain with

both anti-HA and anti-cMyc antibodies led to a markedly increased fluorescence signal that indicates an interaction between Scc1 and Scc3 (Figure 1A and Supplementary Data Set S2). Next, we asked whether incubation of Scc1-6HA Scc3-13cMyc cells with unspecific antibodies might result in fluorescence signal enhancement. To test this, we treated cells with HA-tagged Scc1 and cMyc-tagged Scc3 with anti-HA and anti-Pk antibodies. It turned out that the fluorescence signal was very similar to the signal obtained for other negative controls (Supplementary Figure S2A and Supplementary Data Set S2). We also examined whether incubation with antibodies directed to Pma1, a highly abundant plasma membrane protein, or to an unrelated nuclear protein, Rad53, would result in a fluorescence signal increase. In comparison to other negative controls tested, we observed a stronger fluorescence signal but still much weaker than for the Scc1-6HA Scc3-13cMyc strain incubated with both anti-HA and anti-cMyc antibodies (Supplementary Figure S2B and Supplementary Data Set S2). Finally, we tested whether PLA enables detection of interaction between cohesin and interactors that are not a part of the cohesin complex. We found that PLA allows detection of interactions between Scc1 and Scc2 as well as Scc1 and Sth1, an ATPase subunit of the RSC complex (Supplementary Figure S2C and S2D and Supplementary Data Set S2). Taken together, these data confirm that PLA can be used as a method to detect protein-protein interactions in yeast. Next, we used PLA to examine the interaction between Isw1 and cohesin. To this end, we constructed a strain with Pk-tagged Isw1 and HA-tagged Scc1 and performed PLA. While all negative control experiments resulted in a similar, low fluorescence signal, incubation of Isw1-12Pk Scc1-6HA cells with anti-HA and anti-Pk antibodies resulted in a marked increase of fluorescence intensity, suggesting close proximity of both proteins (Figure 1B and Supplementary Data Set S2). We also determined whether interaction of Isw1 with Scc1 relies on chromatin remodeling activity by performing PLA on a catalytically inactive version of Isw1 with a single amino acid substitution (K227R) (92). It turned out that translocase activity of Isw1 is not essential for Isw1-Scc1 interaction (Figure 1C and Supplementary Data Set S2).

PLA relies on formaldehyde fixation of the cells, which sometimes may lead to unspecific protein binding. Moreover, by using our PLA protocol it cannot be ruled out that the interaction between nuclear proteins is mediated by DNA or RNA. To address these concerns, we performed a CoIP assay on native protein lysates isolated from logarithmically growing cells using protein extracts that were treated with Benzonase and RNase to digest nucleic acids (Supplementary Figure S3A). To validate our assay, we conducted a pull-down experiment using cells that expressed Scc1-6HA and Sth1-12Pk and observed that both proteins interact as previously demonstrated (Supplementary Figure S3B and C) (34,36). Next, we tested Isw1-Scc1 interaction by CoIP. We found that Isw1 co-purifies with Scc1 and, conversely, Scc1 associates with Isw1 (Figure 1D and Supplementary Figure S4A). Scc1 is composed of an N-terminal part that binds to the Smc3 head domain and Pds5, the C-terminus that interacts with the Smc1 head domain and a rather poorly structured middle fragment that is bound by Scc3 (4,5,8,10,22,93). To identify the part of Scc1 to which Isw1 binds, we expressed Isw1-FLAG together with the whole Scc1-cMyc or its truncations (N-Scc1-cMyc, spanning residues 1–120; M-Scc1-cMyc, spanning residues 121–459; C-Scc1-cMyc, spanning residues 460–567) in bacteria. Next, we immunoprecipitated cMyc-tagged proteins and analyzed the eluates by Western blot. We confirmed that Isw1 binds to Scc1. In addition, we found that Isw1 interacts not only with full Scc1 but also with each of the fragments tested (Figure 1E and Supplementary Figure S4B). Finally, we wanted to ascertain whether Isw1-Scc1 interaction takes place in a specific cell cycle phase. To test this, Isw1-12Pk Scc1-6HA cells were synchronized in G1, released into fresh medium and every 15 min a sample was taken for CoIP and FACS. It turned out that Isw1 associates with Scc1 from late G1/early S phase, when Scc1 is resynthesized, to G2 phase (Figure 1F and G, Supplementary Figure S4C). Interestingly, the RSC complex binds also cohesin during S and G2 phase (36). Taken together, these results confirm that Isw1 is a cohesin interactor in yeast.

Isw1 prevents excess cohesin accumulation at CENs and periCENs

Strains lacking genes important for cohesion are characterized by premature sister chromatid separation, so we sought to determine whether cells lacking *ISW1* displays such a phenotype. To this end, we performed a cohesion assay on nocodazole-arrested mitotic cells monitoring SCC at the centromere-proximal *URA3* locus marked with *tetO* or the centromere-distal *LYS4* locus marked with *lacO* repeats. When sister chromatids are tightly cohered, *tetO*/*lacO* arrays coated by TetR-GFP/GFP-LacI, respectively, appear as a single fluorescent dot. Precocious sister chromatid separation is manifested by the appearance of two fluorescent dots (Supplementary Figure S5A) (11,94). We also synchronized cells in G1 with α-factor to exclude the possibility that differences between strains are caused by pre-existing aneuploidy. As a control, we used a strain lacking Ctf18 protein, which promotes cohesin acetylation during S phase contributing to cohesion establishment. As expected, deletion of *CTF18* resulted in a marked increase in premature sister chromatid separation levels at both loci tested (18). On the other hand, *isw1*Δ cells exhibited no cohesion defect at either centromere-proximal *URA3* or centromere-distal *LYS4* loci (Supplementary Figure S5B). This is consistent with a previous report showing a wild-type level of sister chromatid separation in *ISW1*-deficient cells at *URA3* (24). We also tested whether Isw1 is important for SCC at the periCEN of chromosome IV in the presence of a mitotic spindle. As a control, we used a strain lacking Chl4 protein that promotes cohesin loading at CENs. As shown before, *CHL4* deletion resulted in a marked cohesion defect (95). Again, loss of Isw1 did not lead to a cohesion defect at the periCEN of chromosome IV (Supplementary Figure S5C).

To examine whether lack of Isw1 impacts cohesin association with chromatin, we performed calibrated ChIP-seq of Scc1-9Pk using mitotically arrested wild type and *isw1*Δ

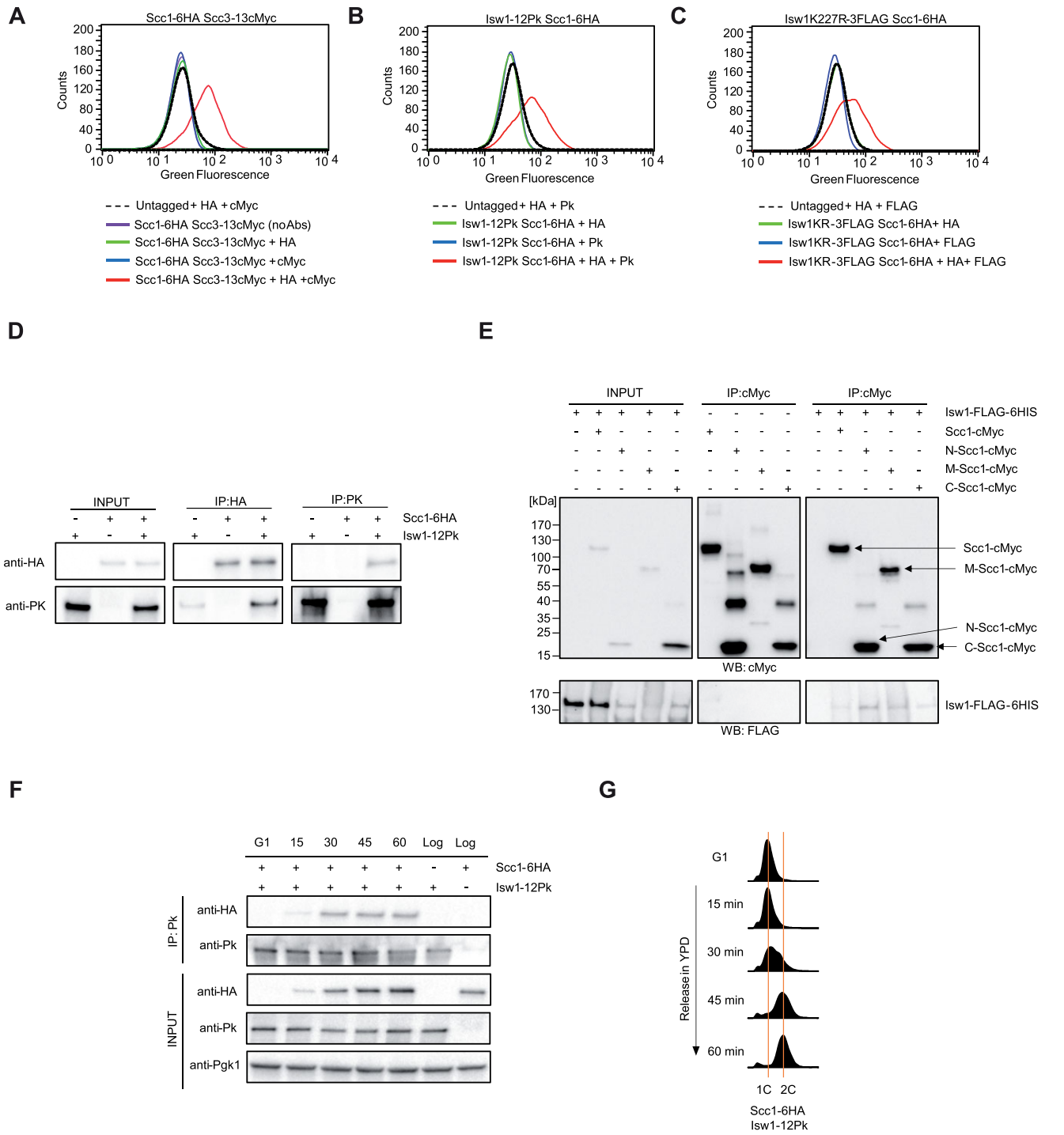

Figure 1. Isw1 physically interacts with cohesin complex. (**A–C**) PLA analysis of interaction between Scc1-6HA and Scc3-18cMyc, Isw1-12Pk and Scc1-6HA and Isw1K227R-3FLAG and Scc1-6HA, respectively. Logarithmically growing cells of indicated yeast strains were fixed with formaldehyde, digested with zymolyase and permeabilized with methanol. Next, cells were incubated overnight with the indicated pair of primary antibodies followed by proximity ligation reaction. (**D**) Coimmunoprecipitation of Isw1-12Pk and Scc1-6HA. Isw1-12Pk and Scc1-6HA were immunoprecipitated with anti-Pk or anti-HA antibody, respectively, and analyzed by Western blot using anti-Pk or anti-HA antibodies. (**E**) Isw1 binds to Scc1 N-terminal, middle and C-terminal fragments. Indicated proteins were expressed in *E. coli* followed by cell lysis. Next, Scc1-cMyc or cMyc-tagged Scc1 fragments were immunoprecipitated with cMyc-nanobodies and analyzed by Western blot using anti-cMyc or anti-FLAG antibodies. (**F**) Isw1-12Pk and Scc1-6HA interact from late G1 to G2/M phase. Isw1-12Pk was immunoprecipitated with anti-Pk antibody and analyzed by Western blot using anti-Pk or anti-HA antibodies. (**G**) Samples of cell cultures used for CoIP in (F) were processed for FACS analysis.

cells (Supplementary Figure S5D). In agreement with previous reports, our analysis showed that in wild type cells a small amount of cohesin associates with chromatin precisely at CENs, while high cohesin levels can be found as a bimodal peak on both sides of CENs and further at periCENs (Figure 2A) (12,65). Surprisingly, loss of *ISW1* resulted in a significant cohesin accumulation at CENs and increased cohesin levels at periCENs (Figure 2A). Closer inspection revealed that elevated cohesin levels could be detected only at pericentromeric regions, which in budding yeast have been estimated recently to span 8.5 kb on average on both sites of CENs (Figure 2B) (33). Moreover, when we analyzed cohesin levels at chromosome arms, we found that the cohesin signal was somewhat reduced in *isw1*Δ cells compared to wild-type (Figure 2C). These data suggest that Isw1 may differentially impact cohesin at CENs and chromosome arms. Although previous data showed that the absence of Isw1 does not significantly change gene expression, we considered the possibility that higher centromeric cohesin levels may result from increased expression of genes encoding cohesin or the cohesin loader. To test this, we monitored *SCC1* and *SCC2* mRNA levels in G2/M synchronized wild type and *isw1*Δ cells. We found no changes in *SCC1* and *SCC2* transcript levels and similar Scc1 and Scc2 protein levels in wild type and *isw1*Δ mutant cells (Supplementary Figure S6A–C). To validate our calibrated ChIP-seq results showing increased cohesin association with CENs and periCENs, we repeated ChIP of Scc1-9Pk on nocodazole arrested cells and employed qPCR for analyses. As a control, we used the yeast strain lacking *CTF18* (Supplementary Figure S5D). Consistent with the cohesion assay, disruption of *CTF18* resulted in decreased cohesin levels at all loci tested. Importantly, in accordance with the ChIP-seq results, ChIP-qPCR revealed increased cohesin accumulation at CENs and periCENs in cells devoid of Isw1 (Figure 2D and E). Next, we asked whether Isw1 translocase activity is required for normal cohesin levels at CENs and periCENs. To this end, we performed ChIP-qPCR of Scc1-9Pk using wild type and *isw1*K227R mutant cells and found a similar increase in cohesin levels as in *isw1*Δ cells (Figure 2D and E, Supplementary Figure S5D). These data indicate that chromatin remodeling activity of Isw1 ensures proper cohesin distribution at CENs and periCENs. We also wondered, whether loss of Chd1, another well-characterized, major nucleosome spacing enzyme in yeast, would lead to a similar phenotype to disruption of *ISW1* (44,45). Interestingly, deletion of *CHD1* had no effect on centromeric cohesin levels (Supplementary Figure S7). Finally, we wondered what would be the consequences of increased cohesin association with CENs and periCENs in cells devoid of Isw1. Since the centromere-bound cohesin must be cleaved in a timely manner by separase to allow for the separation of sister chromatids and mitosis completion, we speculated that more cohesin at CENs may result in mitosis delay (23). To test this hypothesis, wild type and *isw1*Δ cells were arrested in metaphase with nocodazole and then released to fresh medium to analyze chromosome segregation dynamics. It turned out that cells lacking *ISW1* showed significant delay in the completion of mitosis and exhibited a slight increase in generation time (Figure 2F).

ISW1a complex modulates centromeric cohesin levels

In budding yeast, Isw1 ATPase is a part of the ISW1a and ISW1b complexes containing Ioc3 or Ioc2 and Ioc4, respectively (46). These additional subunits direct individual complexes to specific genomic locations and possibly regulate Isw1 activity (46,50–52,96). Taking these data into account, we examined the importance of Ioc subunits for Isw1-Scc1 interaction. To this end, we disrupted ISW1a and ISW1b complexes by deleting *IOC3* and *IOC2* genes, respectively, in the Scc1-6HA Isw1-12Pk background and conducted a CoIP experiment using nocodazole-arrested cells (46). We found that disruption of neither *IOC2* nor *IOC3* abolished Scc1-Isw1 interaction but lack of Ioc3 somewhat reduced it (Figure 3A and Supplementary Figure S8A). These data showed that Isw1 can associate with cohesin as a part of either the ISW1a or the ISW1b complex. Next, we constructed the *ioc2*Δ *ioc3*Δ double mutant and examined Scc1 binding to Isw1. It turned out that very little Scc1 co-purified with Isw1, pointing to a crucial role of Ioc proteins in the Scc1-Isw1 interaction *in vivo* (Figure 3B and Supplementary Figure S8B). Finally, we tested which of the Isw1-containing complexes is important for limiting cohesin accumulation at CENs. The ChIP experiment on mitotically arrested cells revealed that the absence of *IOC3*, but not *IOC2*, caused a similar increase in cohesin levels at CENs as deletion of *ISW1* (Figure 3C and Supplementary Figure S5D). Taken together, these data indicate that while both ISW1a and ISW1b can interact with cohesin, only the ISW1a complex is responsible for regulating cohesin levels at CENs.

Isw1 localizes to CENs

The fact that Isw1 impacts centromeric cohesin levels suggested that it might be present at or near the yeast CENs. Interestingly, SNF2h, the human ortholog of Isw1, was previously shown to localize to CENs, ensuring its stability (97–99). As earlier studies failed to detect Isw1 at CENs, we decided to use different approaches (100). First, we tagged the Cse4 centromere specific histone H3 variant with the HA tag in the Isw1-12Pk background and performed PLA. We detected an increase of fluorescence signal, suggesting close proximity of both proteins (Figure 4A and Supplementary Data Set S2). Next, we repeated the experiment on the Chl4-3HA Isw1-12Pk strain. Again, the result of PLA was positive (Figure 4B and Supplementary Data Set S2). Next, we performed ChIP-qPCR of Isw1-12Pk. Because ChIP of chromatin remodelers (including Isw1) has been repeatedly reported to be intrinsically difficult and inefficient, and since a previous study that employed native ChIP failed to detect Isw1 at CENs, we decided to first stabilize protein-DNA interactions by incubating the cells with formaldehyde and then perform ChIP (51,100–104). Interestingly, we found that Isw1 is present at all three CENs tested (Figure 4C). Next, we asked what the requirements for the recruitment of Isw1 to CENs are. First, we disrupted the CTF19 inner kinetochore subcomplex that supports outer kinetochore assembly and mediates cohesin loading at CENs. It turned out that in the absence of *CTF19* very little Isw1 was present at CENs (Figure 4C). Cbf1 is a basic helix-loop-helix leucine zipper protein that binds the RTCACRTG

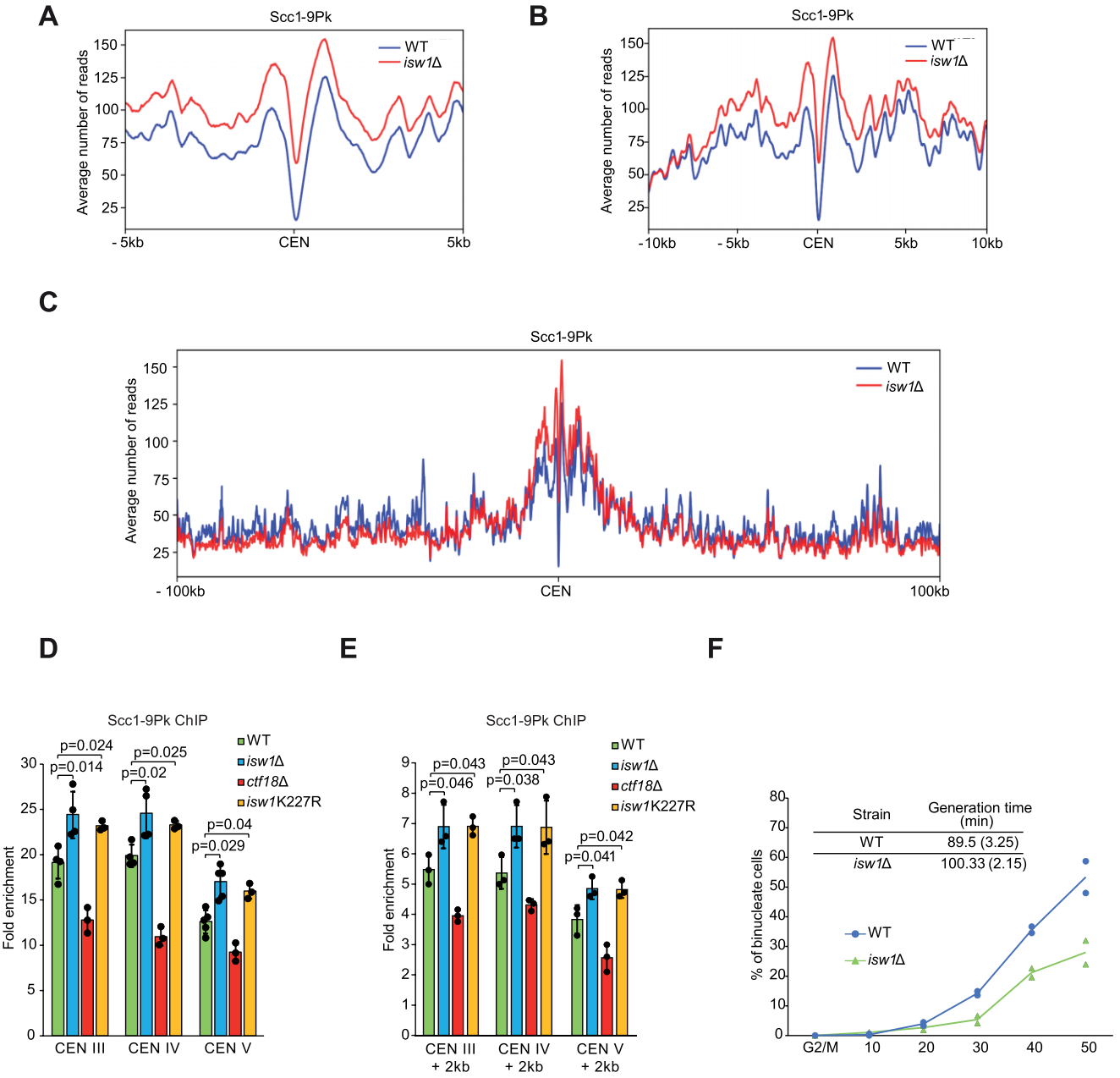

Figure 2. Lack of Isw1 leads to cohesin accumulation at CENs and periCENs. (**A–C**) Average calibrated ChIP-seq profiles of Scc1-9Pk around all budding yeast CENs in wild type and *isw1*Δ cells. (**D**, **E**) ChIP–qPCR analysis of Scc1 association with centromere III, IV and V as well as pericentromeric regions located ∼2 kb from indicated CENs. Error bars represent mean value ± standard deviation of mean. One-way ANOVA was used to calculate the *P*-value. (**F**) Generation time and dynamics of nuclei separation were analyzed in wild type cells and cells lacking *ISW1* ($n = 2$).

(R = A or G) sequence found at the CDEI element of centromeric DNA and certain gene promoters. At the CENs, Cbf1 associates with some kinetochore proteins and regulates the extent and timing of centromeric transcription (105–108). Interestingly, it has been shown that Cbf1 physically interacts with Isw1 and is crucial for its recruitment to *PHO8* and *DRE2* promoters (109,110). Thus, Isw1 could be recruited to the CENs through interaction with Cbf1. However, we found that loss of Cbf1 had no effect on Isw1 occupancy at CENs (Figure 4C). Finally, we tested the importance of Ioc subunits for Isw1 localization to CENs. Interestingly, we found that while deletion of *IOC3* strongly reduced Isw1 association with CENs, lack of *IOC2* increased levels of centromere-bound Isw1. These results suggest that Ioc subunits may compete for binding to Isw1. As a consequence, in the absence of Ioc2, the level of the ISW1a complexes rises, leading to increased ISW1a association with centromeres (Figure 4C). Taken together, these data show that Isw1 localizes to CENs as a part of the ISW1a complex and in a CTF19-dependent fashion.

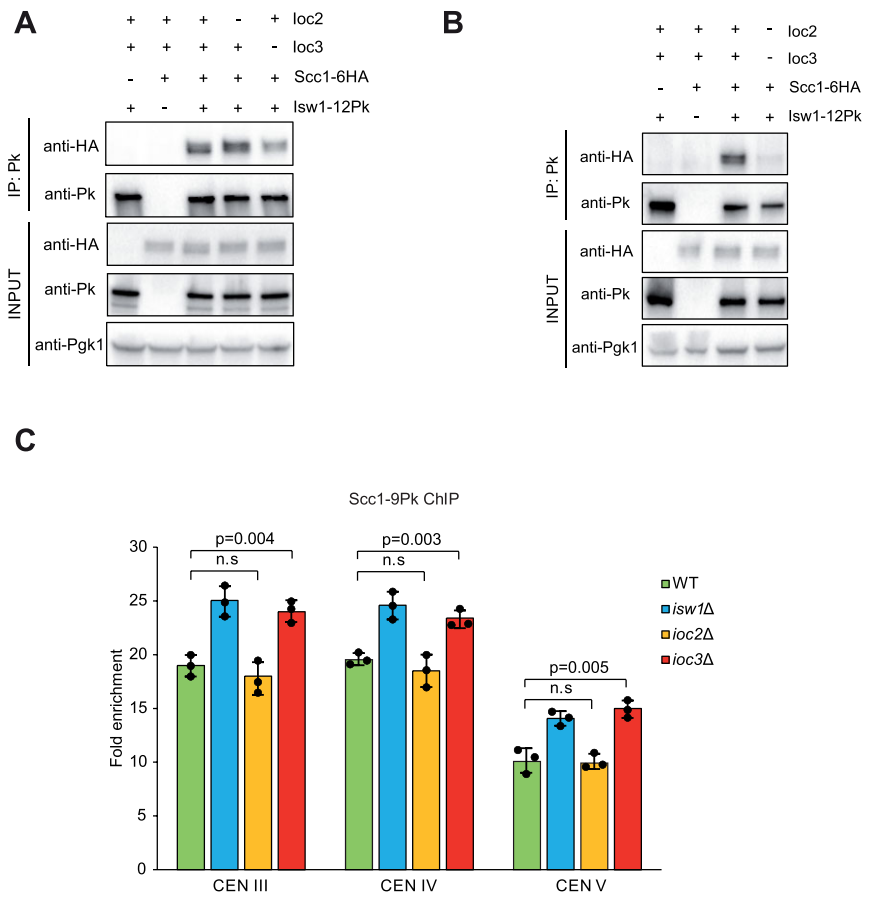

Figure 3. Isw1 in complex with Ioc3 impacts centromeric cohesin levels. (**A**, **B**) Cohesin interacts with both ISW1a and ISW1b. Isw1-12Pk was immunoprecipitated with anti-Pk antibody using protein extracts isolated from wild type, *ioc2*Δ, *ioc3*Δ and *ioc2*Δ *ioc3*Δ cells followed by Western blot analysis using anti-Pk or anti-HA antibodies. (**C**) ChIP–qPCR analysis of Scc1 association with centromere III, IV and V in wild type cells as well as in cells lacking either *IOC2* or *IOC3*. Error bars represent mean value ± standard deviation of mean. One-way ANOVA was used to calculate the P-value.

Isw1 modulates distribution of cohesin loaded by CTF19

In budding yeast, the Ctf19 kinetochore protein recruits the cohesin loader to CENs to ensure high cohesin levels at periCENs (29,95). However, disruption of the CTF19-dependent pathway strongly reduces but does not abolish cohesin association with centromeres. This indicates the existence of another pathway that partially mediates centromeric cohesin enrichment independently of the kinetochore (29,111,112). Taking these results into account, we wondered which of these cohesin loading pathways is important for cohesin enrichment in the absence of Isw1. To test this, we prevented kinetochore-driven cohesin deposition by disrupting *CTF19* or *CHL4*, subunits of the CTF19 complex. As previously reported, this led to a significant reduction in cohesin levels at CENs (Figure 5A) (29,95). Interestingly, while deletion of *ISW1* in otherwise wild type cells resulted in markedly increased cohesin accumulation at CENs, lack of Isw1 in the *ctf19*Δ background had no effect on centromeric cohesin levels (Figure 5A and Supplementary Figure S5D). Consistently, lack of *ISW1* did not alter premature sister chromatid separation observed in *chl4*Δ cells (Figure 5B). Moreover, disruption of *ISW1* neither increased nor attenuated the sensitivity of the CTF19 complex mutants to TBZ, a microtubule poison that sensitizes mutants with impaired centromere or kinetochore functions (Figure 5C and D) (113). These data indicate that cohesin molecules that persist at CENs and periCENs in the absence of Isw1 are loaded by the CTF19 complex.

Isw1 interacts with the cohesin loader complex and impacts its association with CENs and periCENs

In budding yeast, the RSC complex associates with CENs and interacts not only with cohesin but also coprecipitates with cohesin loader subunits *in vivo* (24,34,35). Moreover, recent study claimed that Isw1 also associates with the Scc4 cohesin loader subunit (83). To verify independently the interaction between Isw1 and the Scc2-Scc4 cohesin loader, we first performed CoIP and PLA using Isw1-12Pk Scc2-6HIS-3FLAG cells and found no evidence for an interaction (Supplementary Figure S9A, Supplementary Data Set S2 and data not shown). Next, we asked whether Isw1 binds to Scc4. In agreement with data presented by Muñoz *et al.* (83), we found that Isw1 interacts with Scc4 (Figure 6A and B, Supplementary Figure S9B and Supplementary Data Set S2). Moreover, we also confirmed that the Sth1 subunit of the RSC complex binds Scc4 (Supplementary Figure S9C).

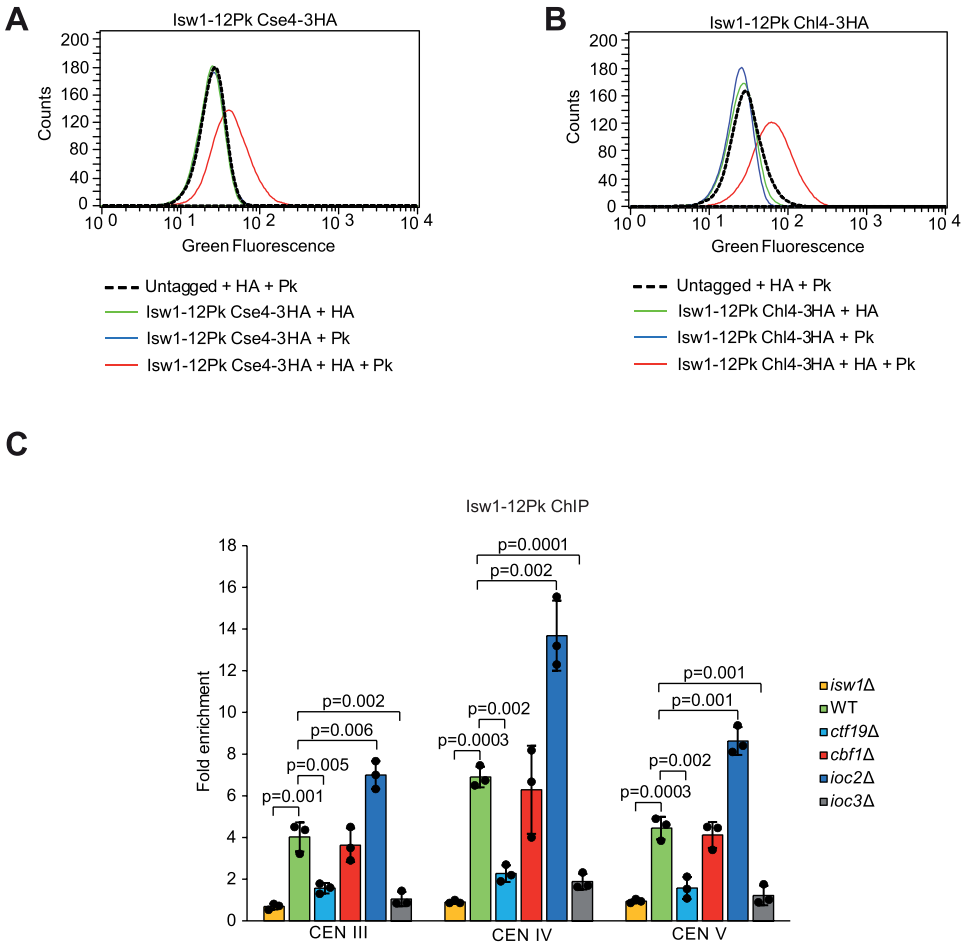

Figure 4. ISW1a binds to CENs. (**A**, **B**) PLA analysis of Isw1-12Pk and Cse4-3HA interaction and Isw1-12Pk and Chl4-3HA interaction. Logarithmically growing cells of indicated yeast strains were fixed with formaldehyde, digested with zymolyase and permeabilized with methanol. Next, cells were incubated overnight with the indicated pair of primary antibodies followed by proximity ligation reaction. (**C**) ChIP–qPCR analysis of Isw1 association with centromere III, IV and V in indicated yeast strains. Error bars represent mean value ± standard deviation of mean. One-way ANOVA was used to calculate the *P*-value.

Next, we decided to examine the importance of the kinetochore-dependent cohesin loading pathway for Isw1-cohesin loader and Isw1-cohesin interaction. For this purpose, we analyzed Scc4 and Scc1 binding to Isw1 in the *ctf19*Δ mutant, which is characterized by low cohesin levels specifically at CENs and periCENs but not along chromosome arms (29,95). We assumed that if Isw1 binds to cohesin at CENs only, disruption of the CTF19-dependent cohesin loading pathway should impair Isw1-Scc4 and Isw1-Scc1 interaction. However, lack of functional CTF19 had no apparent effect on Isw1 association with Scc4 and Scc1 (Figure 6B and C, Supplementary Figure S9B and S9D). Moreover, also Sth1-Scc4 interaction was not reduced in the absence of *CTF19* (Supplementary Figure S9C). These data suggest that the vast majority of Isw1-cohesin loader and Isw1-cohesin interactions takes place elsewhere than at CENs and periCENs.

Increased cohesin levels at CENs and periCENs in *isw1*Δ cells together with our finding that Isw1 associates with Scc4 suggests that Isw1 may impact the function of the cohesin loader. Therefore, we decided to investigate whether Isw1 affects association of the cohesin loader with CENs. To this end, we performed ChIP of the Scc2 cohesin loader subunit from mitotically arrested wild type and *isw1*Δ cells (Supplementary Figure S5D). Interestingly, we found that Scc2 occupancy at three CENs tested was increased in cells lacking *ISW1* (Figure 6D). Also, Scc2 levels at periCENs were increased compared to wild type cells (Figure 6E). Taken together, these data show that *ISW1* disruption increases not only cohesin but also cohesin loader accumulation at CENs and periCENs.

Isw1 impacts nucleosome organization at CENs

Isw1 has been shown to be an important regulator of nucleosomal organization in most budding yeast genes (50,51). As our results indicate that Isw1 is present at CENs (Figure 4), we speculated that it might influence the chromatin landscape at these genomic locations. To test this, we analyzed previously published results of micrococcal nuclease (MNase) digestion and paired-end sequencing of nucleosomal DNA obtained for wild type and *isw1*Δ cells using Danpos software (45,71). First, we used Danpos to analyze nucleosome occupancy of all genes in wild type cells and cells

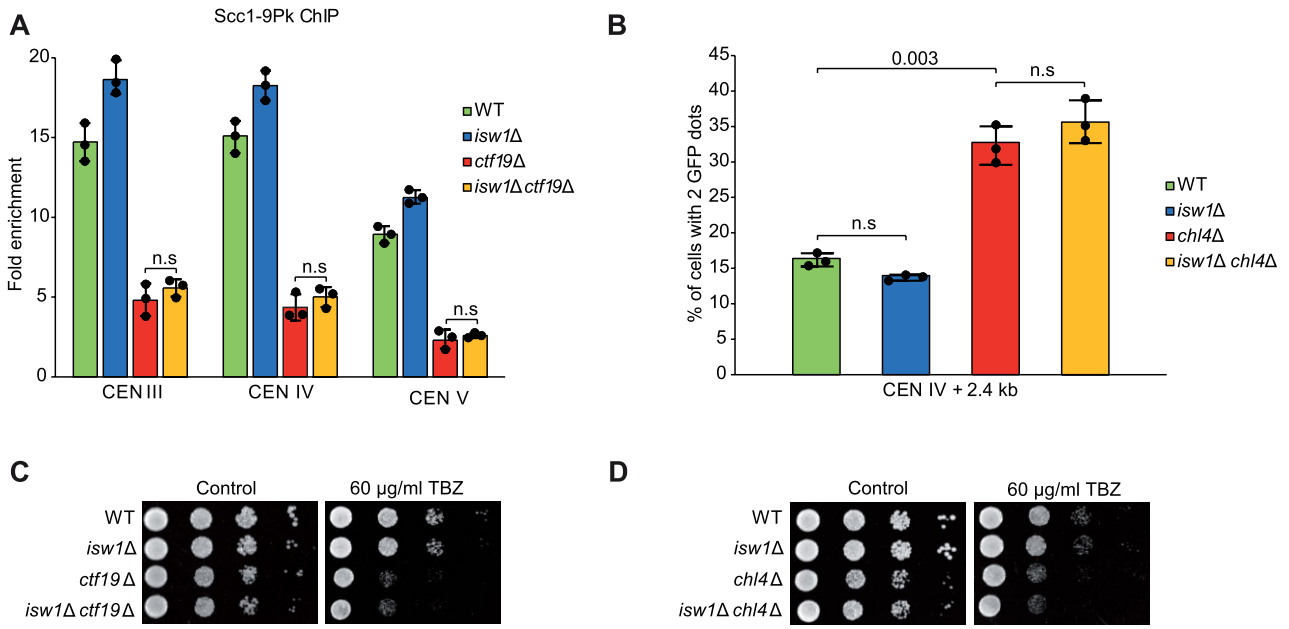

Figure 5. Isw1 modulates chromatin association of cohesin loaded by CTF19. (**A**) ChIP–qPCR analysis of Scc1 association with centromere III, IV and V in wild type, *isw1*Δ, *ctf19*Δ and *isw1*Δ *ctf19*Δ cells. Error bars represent mean value ± standard deviation of mean. One-way ANOVA was used to calculate the P-value. (**B**) Premature sister chromatid separation levels in wild type, *isw1*Δ, *chl4*Δ and *isw1*Δ *chl4*Δ cells. Indicated yeast strains were arrested in G1 with α-factor followed by release into fresh medium containing 8 mM methionine to deplete *CDC20* and arrest cells in G2/M. Next, the number of single or double GFP spots that mark the region ∼2.4 kb from centromere IV were counted. Error bars represent mean value ± standard deviation of mean. (**C**, **D**) Logarithmically growing cultures of indicated strains were 10-fold serially diluted and plated onto solid YPD containing or not containing TBZ.

lacking *ISW1*. A typical yeast gene consists of a nucleosome depleted region (NDR) containing promoter sequences that is flanked by -1 and + 1 nucleosomes. The + 1 nucleosome includes a transcription start site and is followed by subsequent nucleosomes that are regularly phased and spaced, at least to some degree (45,114,115). In agreement with previously published results, our analysis revealed that *ISW1*-deficient cells show weaker nucleosome phasing and shift of the +2 nucleosome as well as downstream nucleosomes towards the promoter (Supplementary Figure S10A) (43,45,101). Next, we analyzed nucleosome occupancy near CENs. As shown previously for wild type cells, CEN nucleosomes were represented by square-shaped peaks rather than round-shaped peaks characteristic for canonical nucleosomes. This indicates that CEN nucleosomes are very well positioned in all cells. Interestingly, the nucleosome occupancy signal for centromeric nucleosomes was markedly lower than for canonical nucleosomes. This suggests that centromeric DNA is more exposed to MNase than DNA wrapped around the averaged canonical nucleosome. All centromeric nucleosomes were adjacent to canonical nucleosomes that were well positioned, possibly reflecting the phasing effect of centromeric nucleosomes. Finally, regions poor in nucleosomes could be found between the CEN nucleosomes and the closest canonical nucleosomes (Figure 7 and Supplementary Figure S10B) (116–120). Close comparison of nucleosome profiles of wild type and *isw1*Δ cells revealed several differences. First, the occupancy signal for centromeric nucleosomes was much stronger when *ISW1* was disrupted (Figure 7 and Supplementary Figure S10B). This indicates that the access of MNase to centromeric DNA is much more restricted when cells lack Isw1. We also observed that in most cases at least one nucleotide poor region flanking CEN nucleosomes was more filled with nucleosomes (Figure 7 and Supplementary Figure S10B). Finally, we analyzed the positioning of canonical nucleosomes located up to 700 bp upstream and downstream from CEN nucleosomes. We found that lack of Isw1 leads to changes in positioning of most canonical nucleosomes but without any obvious pattern (Figure 7 and Supplementary Figure S10B). Because in most cases DNA near CENs includes genes and gene regulatory elements, it is possible that these changes reflect the role of Isw1 in nucleosome organization across gene promoters and gene bodies. However, canonical nucleosomes flanking CEN V showed altered positions, although there are no gene coding or ARS sequences at least 1000 bp upstream and downstream from the centromere (Figure 7). Taken together, these data suggest a role of Isw1 in chromatin organization at CENs and periCENs.

ISW1a balances RSC at centromeres to ensure proper cohesin levels

Recent reports showed that the RSC chromatin remodeler contributes to cohesin loading and that disruption of RSC results in decreased cohesin levels at CENs (24,34). Since Isw1 also regulates cohesin distribution at CENs, we hypothesized that RSC and Isw1 may play distinct roles in cohesin deposition coordination. To test this, we first compared the growth of *rsc2*Δ and *isw1*Δ *rsc2*Δ mutants in the presence of TBZ and observed that deletion of *ISW1* partially rescued *rsc2*Δ sensitivity to TBZ (Figure 8A). This is in agreement with a previous report showing that many phenotypic defects arising from RSC disruption, including

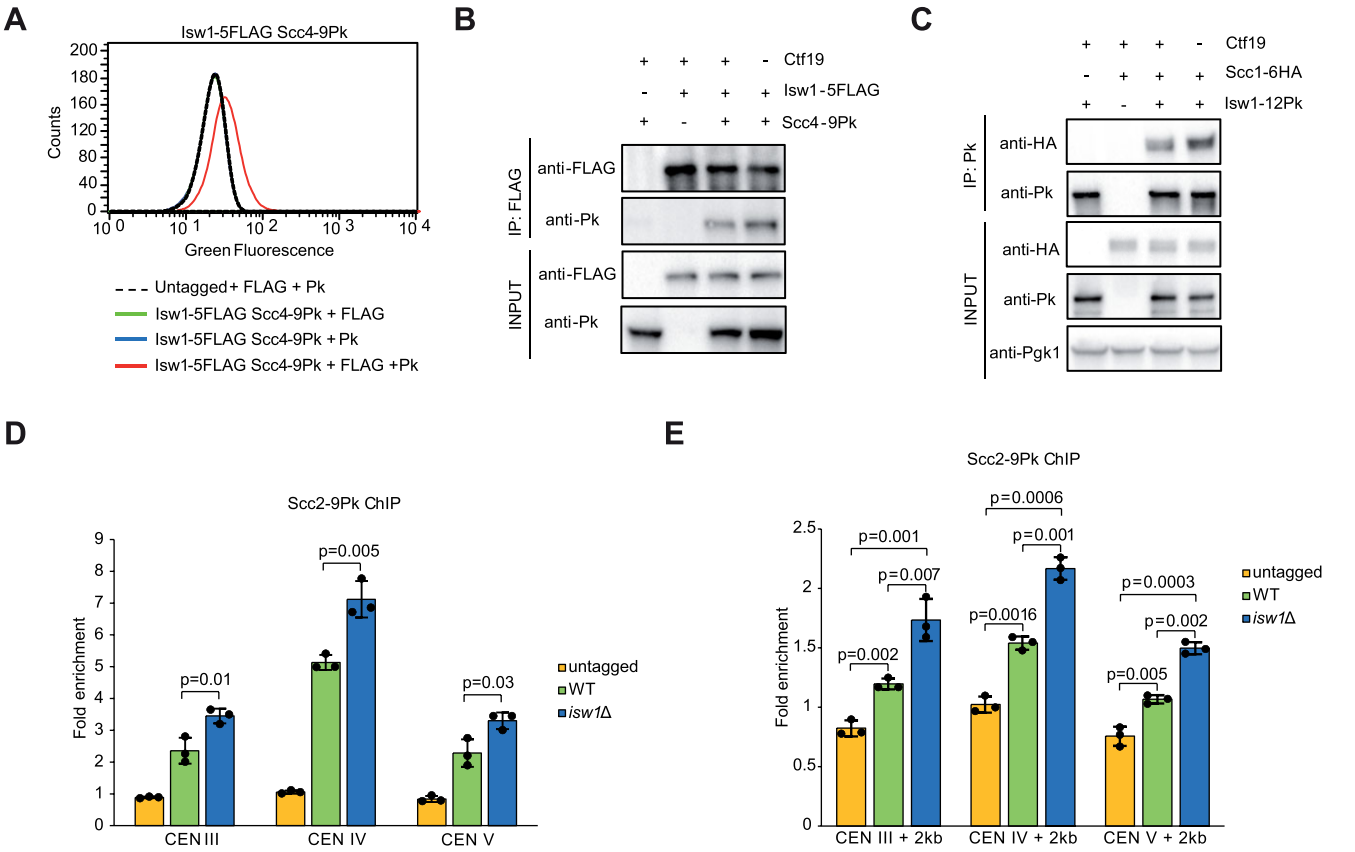

Figure 6. Isw1 influences Scc2 association with chromatin. (**A**) PLA analysis of interaction between Isw1-5FLAG and Scc4-9Pk. Logarithmically growing cells of indicated yeast strains were fixed with formaldehyde, digested with zymolyase and permeabilized with methanol. Next, cells were incubated overnight with the indicated pair of primary antibodies followed by proximity ligation reaction. (**B**) Coimmunoprecipitation analysis of Isw1-Scc4 interaction in wild type and *ctf19*Δ cells. Isw1-5FLAG was immunoprecipitated with anti-FLAG antibody using protein extracts isolated from wild type and *ctf19*Δ cells followed by Western blot analysis using anti-FLAG or anti-Pk antibodies. (**C**) Coimmunoprecipitation analysis of Isw1-Scc1 interaction in wild type and *ctf19*Δ cells. Isw1-12Pk was immunoprecipitated with anti-Pk antibody using protein extracts isolated from wild type and *ctf19*Δ cells followed by Western blot analysis using anti-HA or anti-Pk antibodies. (**D**, **E**) ChIP–qPCR analysis of Scc2 association with CENs and periCENs III, IV and V in untagged, wild type and *isw1*Δ cells. Error bars represent mean value ± standard deviation of mean. One-way ANOVA was used to calculate the P-value.

sensitivity to benomyl, can be attenuated by *ISW1* deletion (101). Additionally, we evaluated the importance of Isw1's translocase activity in suppressing *rsc2*Δ sensitivity to TBZ. It turned out that the catalytically inactive form of Isw1 improved the growth of *rsc2*Δ in the presence of TBZ (Figure 8B). Finally, we wondered which of the Isw1-containing complexes is important for alleviating *rsc2*Δ sensitivity. We found that disruption of ISW1a, but not ISW1b, rescued *rsc2*Δ growth inhibition in the presence of TBZ (Figure 8C). Thus, the stress exerted by TBZ is detrimental for the *rsc2*Δ mutant when ISW1a is present. This epistasis analysis also suggests that Isw1 may counteract RSC binding to chromatin leading to increased TBZ sensitivity when RSC is disrupted. To test this, we performed ChIP of Sth1-12Pk in wild type and *isw1*Δ cells and found no differences in RSC levels between both strains (Supplementary Figure S11). Next, we wondered whether reduction in cohesin levels in *rsc2*Δ cells can be alleviated by *ISW1* loss. To test this, we monitored Scc1-9Pk levels using mitotically arrested *rsc2*Δ and *isw1*Δ *rsc2*Δ cells. Interestingly, disruption of *ISW1* in the *rsc2*Δ background restored cohesin association at all centromeric loci tested to near wild type levels (Figure 8D). Moreover, in agreement with ChIP results, the absence of Isw1 largely improved sister chromatid tethering in *rsc2*Δ cells (Figure 8E). We also analyzed Scc2 association with CENs in *rsc2*Δ and *isw1*Δ *rsc2*Δ mutant cells. It turned out that Scc2 levels also returned to wild type levels in *rsc2*Δ cells in the absence of Isw1 (Figure 8F). These data suggest that the cohesion defect observed in cells with the disrupted RSC complex may be caused by the activity of the ISW1a complex. Finally, we were curious about the relationship between Isw1, RSC and CTF19. To this end, we constructed multiple mutants and performed the growth assay in the presence of TBZ. We found that in the absence of Ctf19, lack of Isw1 no longer rescued *rsc2*Δ mutant sensitivity to TBZ (Figure 8G). Taken together, these data show that functional CTF19, and presumably, cohesin loaded by kinetochore are required for alleviating *rsc2*Δ sensitivity to TBZ by *ISW1* disruption. Furthermore, these results suggest that Isw1 and RSC may have opposite functions at CENs that need to be balanced by mutual chromatin remodeling activity. Loss of balance between these two translocases seems to result in disturbance in cohesin association with CENs.

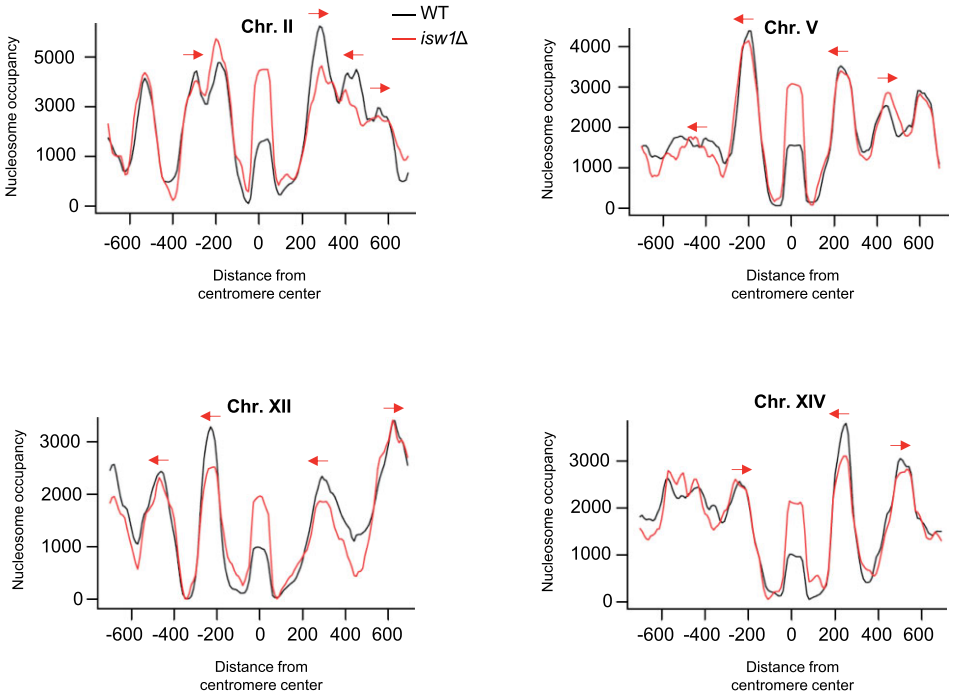

Figure 7. Lack of Isw1 impacts chromatin structure at CENs. Nucleosome occupancy profiles for selected CENs. Centre of centromeric nucleosome was set as 0. Black trace – wild type, red trace – *isw1*Δ. Changes in the position of a CEN-flanking nucleosome dyad peak in *isw1*Δ cells are marked with red arrows. Occupancy profiles for all of the other CENs are presented in Supplementary Figure S10B.

DISCUSSION

In order to better understand how SCC is regulated, we performed a proteomic screen that identified Isw1 chromatin remodeler as a cohesin binding partner (Table 1). Because lack of *ISW1* did not lead to a cohesion defect we asked whether the *isw1*Δ mutation affected the association of cohesin with chromatin (Supplementary Figure S5B and S5C). Surprisingly, we found that in the absence of Isw1, its translocase activity or the Ioc3 regulatory subunit, more rather than less cohesin accumulated at CENs and periCENs (Figure 2A, B, D, E and 3C). Curiously, this is not without precedent, as it has been recently shown that the chromatin remodeler Uls1 restricts cohesin accumulation at the HO-induced DNA double strand break (121,122). Recent ChIP-seq experiments revealed that while large amounts of the cohesin loader associate precisely with CENs, Scc2 is barely detectable along periCENs (12,29). In the case of cohesin, the opposite is true: very little cohesin is associated with CENs, while high levels can be found along periCENs. Current models suggest that Scc2/4 concurrently binds to Ctf19 and the cohesin ring at CENs enabling cohesin to associate with chromatin. Then, it triggers ATP hydrolysis and subsequently dissociates, allowing cohesin to translocate to periCENs (12,29,31). When cohesin is unable to hydrolyze ATP, it cannot translocate and accumulate heavily at CENs together with the cohesin loader. Interestingly, we found that lack of *ISW1* also leads to accumulation of the cohesin loader at CENs (Figure 6D and E). Taking these results into account, our data suggest that ISW1a chromatin remodeling activity is required for proper cohesin translocation from its loading sites at CENs. Moreover, translocation defects most likely lead to partial retention of the cohesin loader and cohesin interaction and colocalization at periCENs (12,65). Accordingly, we found that in the absence of *ISW1*, cohesin and cohesin loader accumulate at periCENs (Figure 2, Figure 3C, Figure 6D and 6E). Increased cohesin levels at periCENs might also arise due limited cohesin turnover because Scc2-bound cohesin is refractory to Wpl1 releasing activity (12). Alternatively, elevated cohesin levels at CENs and periCENs in cells lacking Isw1 could also be explained by enhanced cohesin loading. In this scenario Isw1 would be a factor that restricts cohesin loading possibly by limiting Scc2-Scc4 association with CENs. However, it seems that increased cohesin loading may not coincide with higher levels of Scc2 at CENs and periCENs, as was found for G1-arrested cells lacking Pds5 which inhibits cohesin loading at early stages (12,123). All considered, we favor the notion that Isw1 allows efficient cohesin translocation from loading sites at CENs to its deposition sites at periCENs.

Recent evidence suggests that several chromatin remodelers might physically associate with cohesin loader and cohesin (34,38,82,83). Here, we also observed that Isw1 binds to both complexes. (Figure 1B and D and Figure 6A and B). However, disruption of *CTF19* and thus strong reduction in the centromeric cohesin loader and cohesin levels, had no impact on these interactions when analyzed by CoIP (Figure 6B to E) (29,31). Interestingly, also Sth1-Scc4 interaction was not affected by the *ctf19*Δ mutation despite the fact that disruption of RSC reduces cohesin levels at CENs (24,34) (Supplementary Figure S9C). These data

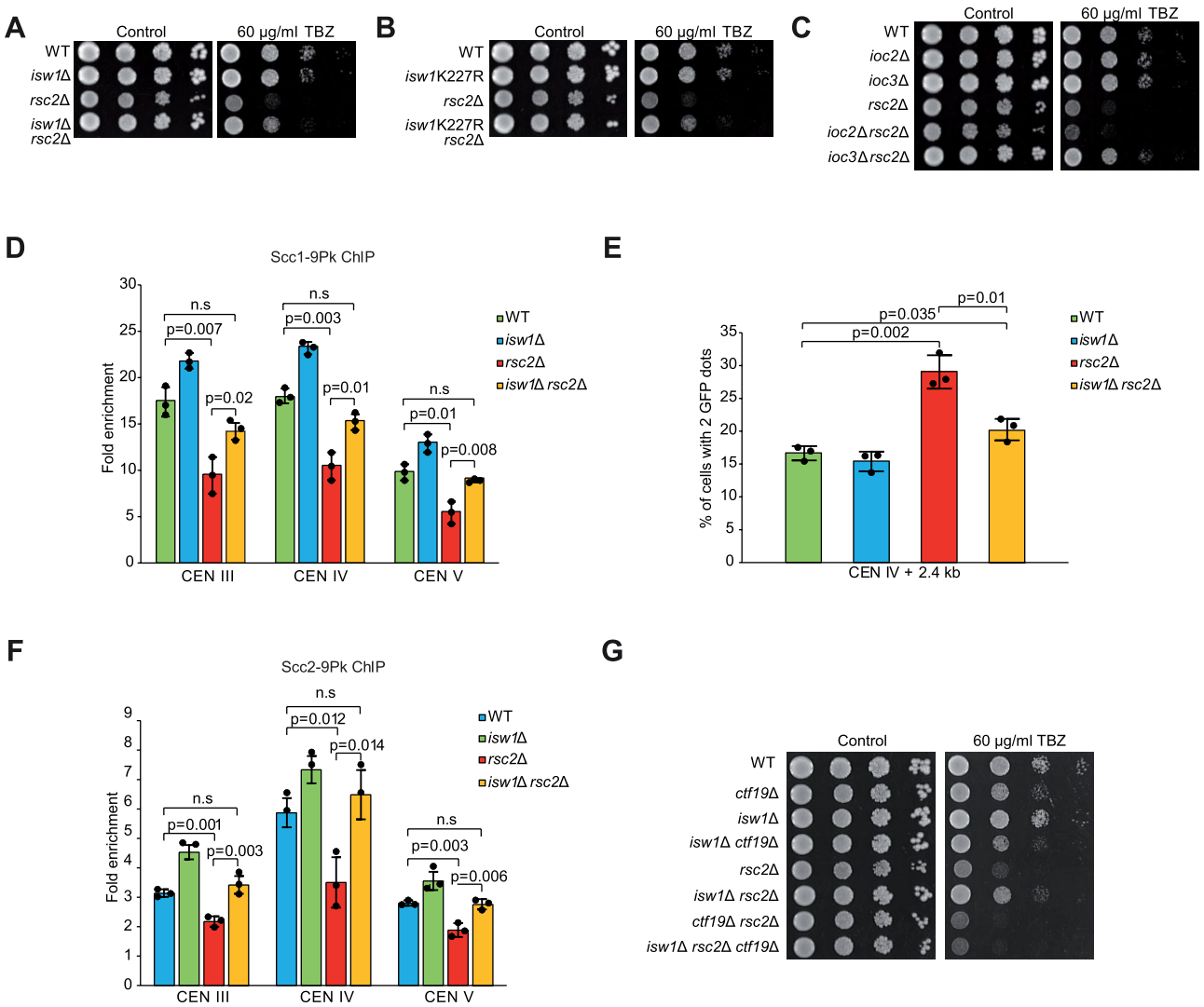

Figure 8. Disruption of Isw1 alleviates cohesion defect of *rsc2*Δ cells. (**A–C**) Logarithmically growing cultures of indicated strains were 10-fold serially diluted and plated onto solid YPD containing or not containing TBZ. (**D**) ChIP–qPCR analysis of Scc1 association with centromere III, IV and V in wild type, *isw1*Δ, *rsc2*Δ and *isw1*Δ *rsc2*Δ cells. Error bars represent mean value ± standard deviation of mean. One-way ANOVA was used to calculate the *P*-value. (**E**) Premature sister chromatid separation levels in wild type, *isw1*Δ, *rsc2*Δ and *isw1*Δ *rsc2*Δ cells. Indicated yeast strains were arrested in G1 with α-factor followed by release into fresh medium containing 8 mM methionine to deplete *CDC20* and arrest cells in G2/M. Next, the number of single or double GFP spots that mark the region ∼2.4 kb from centromere IV were counted. Error bars represent mean value ± standard deviation of mean. (**F**) ChIP–qPCR analysis of Scc2 association with centromere III, IV and V in wild type, *isw1*Δ, *rsc2*Δ and *isw1*Δ *rsc2*Δ cells. Error bars represent mean value ± standard deviation of mean. One-way ANOVA was used to calculate the *P*-value. (**G**) Logarithmically growing cultures of indicated strains were 10-fold serially diluted and plated onto solid YPD containing or not containing TBZ.

suggest that most of the Isw1-cohesin loader and Isw1-cohesin interactions take place on chromosome arms. Nevertheless, we found that the presence of intact CTF19 is required for Isw1 localization at CENs, where it presumably colocalizes with Scc2/4 and cohesin (Figure 4C). Taking the evidence together, we propose that a fraction of Isw1 binds to cohesin and cohesin loader associated with CENs enabling efficient cohesin translocation to periCENs. Nonetheless, it seems that Isw1 has a role in cohesin association with chromosome arms. It was previously suggested that chromatin remodelers such as Isw1 or Chd1 might work as chromatin receptors that recruit the cohesin loader (34). Interestingly, ChIP-seq analysis revealed that in contrast to CENs, cohesin levels at chromosome arms were slightly reduced in *isw1*Δ cells (Figure 2C). This reduction is likely too small to cause a global cohesion defect especially since nucleosome spacing chromatin remodelers largely compensate for mutual losses (44–46,124,125). Moreover, our research showed that cohesin interacts with both Isw1-containing complexes and that the presence of Ioc subunits is crucial for these interactions (Figure 3A and B). Whole genome mapping experiments revealed that both ISW1a and ISW1b are present at many genes and bind to most of the gene sequence from the +1 nucleosome to the terminal nucleosomes where cohesin often accumulates (51). Importantly, cohesin loading

onto chromosome arms seems to predominantly take place at gene promoters but it appears that it might also occur uniformly across transcription units (12,24,25,65). These data indicate that Isw1 complexes, the cohesin loader and cohesin occupy similar locations giving opportunities for interaction.

Our study provides evidence that Isw1 localizes to CENs, where it utilizes its chromatin remodeling activity to modulate cohesin association with chromatin (Figures 2 and 4). Because Isw1 is one of the major proteins that regulate nucleosome spacing in budding yeast, one might suppose that it contributes to cohesin translocation by influencing the chromatin landscape at and/or around the centromere. However, how chromatin organization impacts cohesin loading and translocation is not well understood. Scc2 is a DNA binding protein with affinity to both single stranded and double stranded DNA. Accordingly, a recent study showed that substitution of Scc2 residues implicated in DNA binding causes strong reduction of cohesin's association with chromatin (17). Next, cohesin loading requires an entry point through which cohesin accesses DNA. It seems that at least *in vitro* naked DNA is a better substrate for cohesin loading than chromatinized DNA. This may explain why cohesin loading along chromosome arms seems to preferentially take place at promoters that are often poorly covered with nucleosomes (24,25,34). In vivo, weaker association between histones and DNA, and thus most likely better accessibility of DNA, seem to improve cohesin association along chromosomes arms (126). Taken together, these results imply that the presence and extent of unchromatinized DNA might be crucial for cohesin deposition and translocation.

Interestingly, histone-depleted regions flank CEN nucleosomes, making them possible candidate regions for cohesin loading and starting-points for cohesin translocation to periCENs (116,117). However, our nucleosome occupancy analysis revealed that cohesin retention at CENs in *isw1*Δ cells does not correlate with widening of this region; instead we observed its mild filling (Figure 7 and Supplementary Figure S10B). These data suggest that histone-depleted regions flanking CEN nucleosomes are not the regions where cohesin is loaded and start to translocate or the presence of nucleosomes is not inhibitory for these reactions at CENs. The latter conclusion is in agreement with a previous report showing that disruption of chromatin integrity by partial histone depletion does not generally affect cohesin association with CENs (80). We also found that lack of Isw1 results in position changes of canonical nucleosomes near CEN nucleosomes (Figure 7 and Supplementary Figure S10B). This raises a possibility that Isw1 may specifically influence the pattern of nucleosomes around CENs and that positioning of these nucleosomes may enable efficient cohesin translocation. This would be somewhat reminiscent of replication origins where NDRs are flanked by phased arrays of regularly spaced nucleosomes formed by chromatin remodelers including ISW1a. There, disruption of nucleosome organization around replication origins hinders DNA replication (125). Finally, we observed that deletion of *ISW1* led to an increased occupancy signal for centromeric nucleosomes, which in wild type cells is very low due to its high accessibility for MNase (Figure 7 and Supplementary Figure S10B) (116,118,119). As MNase digests preferentially at sites centered on A/T-containing dinucleotides, the increased signal for CEN nucleosomes in *isw1*Δ cells may indicate that the AT-rich CDEII element of centromeric DNA is specifically inaccessible to MNase (127–129). Alternatively, centromeric DNA of cells lacking *ISW1* may be protected by some protein barrier that largely precludes MNase accession. Whether and how it influences cohesin loading and/or translocation remains to be established, however, it is tempting to speculate that centromeric DNA that is more tightly wrapped around the Cse4-containing nucleosome provides a suboptimal start point these processes. Interestingly, recent data suggest that cohesin loader-RSC physical interaction stimulates nucleosome sliding activity of the RSC complex *in vitro*. Moreover, this study identified a FEDWF motif in Sth1 that seems to be crucial for RSC association with the cohesin loader. Importantly, this motif is present in most Snf2-like ATPases, including Isw1 (83). This raises a possibility that the cohesin loader bound to the cohesin complex may attract different chromatin remodelers, driving its remodeling activity and allowing efficient translocation and/or bypassing of different barriers including nucleosomes which hinder cohesin diffusion *in vitro* (130). Taken together, these data indicate that accurate organization of nucleosome arrays around CENs is important for proper cohesion.

Chromatin remodelers are the key enzymes in the cell that govern nucleosome occupancy, position and structure, thus regulating many chromatin transactions, including gene expression. Interestingly, at some promoters RSC and Isw1 have opposing functions: while RSC prevents encroachment of -1 and + 1 nucleosomes into the NDR, ISW1a shifts + 1 nucleosomes towards NDR. Consequently, while lack of functional RSC results in narrowing and filling of the NDR, disruption of ISW1a in the *rsc* mutant background partially reverses this effect, leading to improved growth under normal and stress conditions (51,101). Intriguingly, deletion of *ISW1* in *rsc2*Δ cells restored cohesin and cohesin loader binding to CENs and improved centromeric cohesion (Figure 8D–F). These data suggest that one of the roles of Isw1 at CENs is to balance RSC activity. Thus, it seems that, as in the case of promoters, also at CENs, chromatin remodelers compete to establish a certain chromatin environment.

In recent years, much progress has been made in understanding the SCC process. It has become clear that SWI/SNF family proteins play an important role in regulation of cohesion not only in yeast but also in higher eukaryotes. Chromatin remodelers such as PBAF, ATRX or human ortholog of Isw1, SNF2H, have been shown to interact with cohesin and to regulate cohesin association with chromatin (131–135). As mutations in cohesin, cohesin regulators and chromatin remodelers are present in many cancers and are the underlying cause of several developmental disorders, further investigation exploring the interplay between these factors is of great importance (136–141).

DATA AVAILABILITY

Strains and plasmids are available upon request. The mass spectrometry proteomics data have been deposited

in the ProteomeXchange Consortium via the PRIDE partner repository with the dataset identifier PXD037034 and 10.6019/PXD037034. Sequencing datasets are available at the Gene Expression Omnibus (GEO; https://www.ncbi.nlm.nih.gov/geo/), accession number GSEGSE232315.

SUPPLEMENTARY DATA

Supplementary Data are available at NAR Online.

ACKNOWLEDGEMENTS

We thank Jennifer Cobb, Adele Marston, Lena Ström, Doug Koshland, Rodney Rothstein, Toshio Tsukiyama and Frank Uhlmann for providing yeast strains, Ramon Serrano for anti-Pma1 antibodies, Wojciech Białek for help with the pull-down assay in *E. coli* and Ewa Pilarczyk for initial work in this project.

FUNDING

This work was supported by a National Science Centre (Poland) grant (2018/31/B/NZ2/00337) to I.L.; K.K. was supported by the program 'Excellence Initiative - Research University' for the University of Wrocław of the Ministry of Education and Science from Poland (IDN.CBNDR 0320/2020/20); the equipment used for MS analysis at the Mass Spectrometry Laboratory, Institute of Biochemistry and Biophysics PAS was sponsored in part by the Centre for Preclinical Research and Technology (CePT), a project co-sponsored by the European Regional Development Fund and Innovative Economy, the National Cohesion Strategy of Poland. Funding for open access charge: Open access charge was financially supported by the Excellence Initiative-Research University (IDUB) program for the University of Wroclaw.
Conflict of interest statement. None declared.

REFERENCES

1. Nasmyth,K. (2001) Disseminating the genome: joining, resolving, and separating sister chromatids during mitosis and meiosis. *Annu. Rev. Genet.*, **35**, 673–745.
2. Potapova,T. and Gorbsky,G.J. (2017) The consequences of chromosome segregation errors in mitosis and meiosis. *Biology (Basel)*, **6**, 12.
3. Ly,P., Brunner,S.F., Shoshani,O., Kim,D.H., Lan,W., Pyntikova,T., Flanagan,A.M., Behjati,S., Page,D.C., Campbell,P.J. *et al.* (2019) Chromosome segregation errors generate a diverse spectrum of simple and complex genomic rearrangements. *Nat. Genet.*, **51**, 705–715.
4. Haering,C.H., Farcas,A.-M., Arumugam,P., Metson,J. and Nasmyth,K. (2008) The cohesin ring concatenates sister DNA molecules. *Nature*, **454**, 297–301.
5. Gligoris,T.G., Scheinost,J.C., Bürmann,F., Petela,N., Uluocak,P., Beckouët,F., Gruber,S. and Nasmyth,K. (2015) Closing the cohesin ring : structure and function of its Smc3- kleisin interface. *Science*, **346**, 963–967.
6. Kulemzina,I., Schumacher,M.R., Verma,V., Reiter,J., Metzler,J., Failla,A.V., Lanz,C., Sreedharan,V.T., Rätsch,G. and Ivanov,D. (2012) Cohesin rings devoid of Scc3 and Pds5 maintain their stable association with the DNA. *PLoS Genet*, **8**, e1002856.
7. Chatterjee,A., Zakian,S., Hu,X.W. and Singleton,M.R. (2013) Structural insights into the regulation of cohesion establishment by Wpl1. *EMBO J.*, **32**, 677–687.
8. Haering,C.H., Lö,J., Hochwagen,A. and Nasmyth,K. (2002) Molecular architecture of SMC proteins and the yeast cohesin complex. *Mol. Cell*, **9**, 773–788.
9. Muir,K.W., Kschonsak,M., Li,Y., Metz,J., Haering,C.H. and Panne,D. (2016) Structure of the Pds5-Scc1 complex and implications for cohesin function. *Cell Rep.*, **14**, 2116–2126.
10. Musacchio,A., Li,Y., Muir,K.W., Bowler,M.W., Metz,J., Haering,C.H. and Panne,D. (2018) Structural basis for Scc3-dependent cohesin recruitment to chromatin. *Elife*, **15**, e38356.
11. Michaelis,C., Ciosk,R. and Nasmyth,K. (1997) Cohesins: chromosomal proteins that prevent premature separation of sister chromatids. *Cell*, **91**, 35–45.
12. Petela,N.J., Gligoris,T.G., Metson,J., Lee,B.G., Voulgaris,M., Hu,B., Kikuchi,S., Chapard,C., Chen,W., Rajendra,E. *et al.* (2018) Scc2 is a potent activator of cohesin's ATPase that promotes loading by binding Scc1 without Pds5. *Mol. Cell*, **70**, 1134–1148.
13. Ciosk,R., Shirayama,M., Shevchenko,A., Tanaka,T., Toth,A., Shevchenko,A. and Nasmyth,K. (2000) Cohesin's binding to chromosomes depends on a separate complex consisting of Scc2 and Scc4 proteins. *Mol. Cell*, **5**, 243–254.
14. Murayama,Y. and Uhlmann,F. (2014) Biochemical reconstitution of topological DNA binding by the cohesin ring. *Nature*, **505**, 367–371.
15. Elbatsh,A.M.O., Haarhuis,J.H.I., Petela,N., Chapard,C., Fish,A., Celie,P.H., Stadnik,M., Ristic,D., Wyman,C., Medema,R.H. *et al.* (2016) Cohesin releases DNA through asymmetric ATPase-driven ring opening. *Mol. Cell*, **61**, 575–588.
16. Murayama,Y. and Uhlmann,F. (2015) DNA entry into and exit out of the cohesin ring by an interlocking gate mechanism. *Cell*, **163**, 1628–1640.
17. Kurokawa,Y. and Murayama,Y. (2020) DNA binding by the Mis4/Scc2 loader promotes topological DNA entrapment by the cohesin ring. *Cell Rep.*, **33**, 108357.
18. Liu,H.W., Bouchoux,C., Panarotto,M., Kakui,Y., Patel,H. and Uhlmann,F. (2020) Division of labor between PCNA loaders in DNA replication and sister chromatid cohesion establishment. *Mol. Cell*, **78**, 725–738.
19. Zhang,J., Shi,X., Li,Y., Kim,B.J., Jia,J., Huang,Z., Yang,T., Fu,X., Jung,S.Y., Wang,Y. *et al.* (2008) Acetylation of Smc3 by Eco1 is required for S phase sister chromatid cohesion in both human and yeast. *Mol. Cell*, **31**, 143–151.
20. Moldovan,G.L., Pfander,B. and Jentsch,S. (2006) PCNA controls establishment of sister chromatid cohesion during S phase. *Mol. Cell*, **23**, 723–732.
21. Chan,K.L., Gligoris,T., Upcher,W., Kato,Y., Shirahige,K., Nasmyth,K. and Beckouët,F. (2013) Pds5 promotes and protects cohesin acetylation. *Proc. Natl. Acad. Sci. U.S.A.*, **110**, 13020–13025.
22. Roig,M.B., Löwe,J., Chan,K.L., Beckouët,F., Metson,J. and Nasmyth,K. (2014) Structure and function of cohesin's Scc3/SA regulatory subunit. *FEBS Lett.*, **588**, 3692–3702.
23. Uhlmann,F., Lottspeich,F. and Nasmyth,K. (1999) Sister-chromatid separation at anaphase onset is promoted by cleavage of the cohesin subunit Scc1. *Nature*, **400**, 37–42.
24. Lopez-Serra,L., Kelly,G., Patel,H., Stewart,A. and Uhlmann,F. (2014) The Scc2–Scc4 complex acts in sister chromatid cohesion and transcriptional regulation by maintaining nucleosome-free regions. *Nat. Genet.*, **46**, 1147–1151.
25. Lengronne,A., Katou,Y., Mori,S., Yokobayashi,S., Kelly,G.P., Itoh,T., Watanabe,Y., Shirahige,K. and Uhlmann,F. (2004) Cohesin relocation from sites of chromosomal loading to places of convergent transcription. *Nature*, **430**, 573–578.
26. Ocampo-Hafalla,M., Muñoz,S., Samora,C.P. and Uhlmann,F. (2016) Evidence for cohesin sliding along budding yeast chromosomes. *Open Biol.*, **6**, 150178.
27. Biggins,S. (2013) The composition, functions, and regulation of the budding yeast kinetochore. *Genetics*, **194**, 817–846.
28. Fischböck-Halwachs,J., Singh,S., Potocnjak,M., Hagemann,G., Solis-Mezarino,V., Woike,S., Ghodgaonkar-Steger,M., Weissmann,F., Gallego,L.D., Rojas,J. *et al.* (2019) The COMA complex interacts with Cse4 and positions Sli15/Ipl1 at the budding yeast inner kinetochore. *Elife*, **8**, e42879.
29. Hinshaw,S.M., Makrantoni,V., Harrison,S.C. and Marston,A.L. (2017) The kinetochore receptor for the cohesin loading complex. *Cell*, **171**, 72–84.

30. Weber,S.A., Gerton,J.L., Polancic,J.E., DeRisi,J.L., Koshland,D. and Megee,P.C. (2004) The kinetochore is an enhancer of pericentric cohesin binding. *PLoS Biol.*, **2**. E260.
31. Fernius,J., Nerusheva,O.O., Galander,S., Alves,F.D.L., Rappsilber,J. and Marston,A.L. (2013) Cohesin-dependent association of Scc2/4 with the centromere initiates pericentromeric cohesion establishment. *Curr. Biol.*, **23**, 599–606.
32. Garcia-Luis,J., Lazar-Stefanita,L., Gutierrez-Escribano,P., Thierry,A., Cournac,A., García,A., González,S., Sánchez,M., Jarmuz,A., Montoya,A. *et al.* (2019) FACT mediates cohesin function on chromatin. *Nat. Struct. Mol. Biol.*, **26**, 970–979.
33. Paldi,F., Alver,B., Robertson,D., Schalbetter,S.A., Kerr,A., Kelly,D.A., Baxter,J., Neale,M.J. and Marston,A.L. (2020) Convergent genes shape budding yeast pericentromeres. *Nature*, **582**, 119–123.
34. Muñoz,S., Minamino,M., Casas-Delucchi,C.S., Patel,H. and Uhlmann,F. (2019) A role for chromatin remodeling in cohesin loading onto chromosomes. *Mol. Cell*, **74**, 664–673.
35. Hsu,J., Huang,J., Meluh,P.B. and Laurent,B.C. (2003) The yeast RSC chromatin-remodeling complex is required for kinetochore function in chromosome segregation. *Mol. Cell Biol.*, **23**, 3202–3215.
36. Huang,J., Hsu,J.M. and Laurent,B.C. (2004) The RSC nucleosome-remodeling complex is required for cohesin's association with chromosome arms. *Mol. Cell*, **13**, 739–750.
37. Baetz,K.K., Krogan,N.J., Emili,A., Greenblatt,J. and Hieter,P. (2004) The ctf13-30/CTF13 genomic haploinsufficiency modifier screen identifies the yeast chromatin remodeling complex RSC, which is required for the establishment of sister chromatid cohesion. *Mol. Cell Biol.*, **24**, 1232–1244.
38. Litwin,I., Bakowski,T., Maciaszczyk-Dziubinska,E. and Wysocki,R. (2017) The LSH/HELLS homolog Irc5 contributes to cohesin association with chromatin in yeast. *Nucleic Acids Res.*, **45**, 6404–6416.
39. Boginya,A., Detroja,R., Matityahu,A., Frenkel-Morgenstern,M. and Onn,I. (2019) The chromatin remodeler Chd1 regulates cohesin in budding yeast and humans. *Sci. Rep.*, **9**, 8929.
40. Chen,Y.F., Chou,C.C. and Gartenberg,M.R. (2016) Determinants of Sir2-mediated, silent chromatin cohesion. *Mol. Cell Biol.*, **36**, 2039–2050.
41. Paul,S. and Bartholomew,B. (2018) Regulation of ATP-dependent chromatin remodelers: accelerators/brakes, anchors and sensors. *Biochem. Soc. Trans.*, **46**, 1423–1430.
42. Clapier,C.R., Iwasa,J., Cairns,B.R. and Peterson,C.L. (2017) Mechanisms of action and regulation of ATP-dependent chromatin-remodelling complexes. *Nat. Rev. Mol. Cell Biol.*, **18**, 407–422.
43. Gkikopoulos,T., Schofield,P., Singh,V., Pinskaya,M., Mellor,J., Smolle,M., Workman,J.L., Barton,G.J. and Owen-Hughes,T. (2011) A role for Snf2-related nucleosome-spacing enzymes in genome-wide nucleosome organization. *Science*, **333**, 1758–1760.
44. Ocampo,J., Chereji,R.V., Eriksson,P.R. and Clark,D.J. (2019) Contrasting roles of the RSC and ISW1/CHD1 chromatin remodelers in RNA polymerase II elongation and termination. *Genome Res.*, **29**, 407–417.
45. Ocampo,J., Chereji,R.V., Eriksson,P.R. and Clark,D.J. (2016) The ISW1 and CHD1 ATP-dependent chromatin remodelers compete to set nucleosome spacing in vivo. *Nucleic Acids Res.*, **44**, 4625–4635.
46. Vary,J.C., Gangaraju,V.K., Qin,J., Landel,C.C., Kooperberg,C., Bartholomew,B. and Tsukiyama,T. (2003) Yeast Isw1p forms two separable complexes in vivo. *Mol. Cell Biol.*, **23**, 80–91.
47. Lenstra,T.L., Benschop,J.J., Kim,T.S., Schulze,J.M., Brabers,N.A.C.H., Margaritis,T., van de Pasch,L.A.L., van Heesch,S.A.A.C., Brok,M.O., Groot Koerkamp,M.J.A. *et al.* (2011) The specificity and topology of chromatin interaction pathways in yeast. *Mol. Cell*, **42**, 536–549.
48. Tirosh,I., Sigal,N. and Barkai,N. (2010) Widespread remodeling of mid-coding sequence nucleosomes by Isw1. *Genome Biol.*, **11**, R49.
49. Lindstrom,K.C., Vary,J.C., Parthun,M.R., Delrow,J. and Tsukiyama,T. (2006) Isw1 functions in parallel with the Nua4 and Swr1 complexes in stress-induced gene repression. *Mol. Cell Biol.*, **26**, 6117–6129.
50. Smolle,M., Venkatesh,S., Gogol,M.M., Li,H., Zhang,Y., Florens,L., Washburn,M.P. and Workman,J.L. (2012) Chromatin remodelers Isw1 and Chd1 maintain chromatin structure during transcription by preventing histone exchange. *Nat. Struct. Mol. Biol.*, **19**, 884–892.
51. Yen,K., Vinayachandran,V., Batta,K., Koerber,R.T. and Pugh,B.F. (2012) Genome-wide nucleosome specificity and directionality of chromatin remodelers. *Cell*, **149**, 1461–1473.
52. Bhardwaj,S.K., Hailu,S.G., Olufemi,L., Brahma,S., Kundu,S., Hota,S.K., Persinger,J. and Bartholomew,B. (2020) Dinucleosome specificity and allosteric switch of the ISW1a ATP-dependent chromatin remodeler in transcription regulation. *Nat. Commun.*, **11**, 5913.
53. Gadaleta,M.C., Iwasaki,O., Noguchi,C., Noma,K.I. and Noguchi,E. (2013) New vectors for epitope tagging and gene disruption in *Schizosaccharomyces pombe*. *Biotechniques*, **55**, 257–263.
54. Goldstein,A.L. and McCusker,J.H. (1999) Three new dominant drug resistance cassettes for gene disruption in *Saccharomyces cerevisiae*. *Yeast*, **15**, 1541–1553.
55. Longtine,M.S., Mckenzie,A. III, Demarini,D.J., Shah,N.G., Wach,A., Brachat,A., Philippsen,P. and Pringle,J.R. (1998) Additional modules for versatile and economical PCR-based gene deletion and modification in *Saccharomyces cerevisiae*. *Yeast*, **14**, 953–961.
56. Hentges,P., van Driessche,B., Tafforeau,L., Vandenhaute,J. and Carr,A.M. (2005) Three novel antibiotic marker cassettes for gene disruption and marker switching in *Schizosaccharomyces pombe*. *Yeast*, **22**, 1013–1019.
57. Shah,P.P., Zheng,X., Epshtein,A., Carey,J.N., Bishop,D.K. and Klein,H.L. (2010) Swi2/Snf2-related translocases prevent accumulation of toxic Rad51 complexes during mitotic growth. *Mol. Cell*, **39**, 862–872.
58. Lambert,J.P., Fillingham,J., Siahbazi,M., Greenblatt,J., Baetz,K. and Figeys,D. (2010) Defining the budding yeast chromatin-associated interactome. *Mol. Syst. Biol.*, **6**. 448.
59. Breitkreutz,A., Choi,H., Sharom,J.R., Boucher,L., Neduva,V., Larsen,B., Lin,Z.Y., Breitkreutz,B.J., Stark,C., Liu,G. *et al.* (2010) A global protein kinase and phosphatase interaction network in yeast. *Science*, **328**, 1043–1046.
60. Jiang,H., Lei,R., Ding,S.W. and Zhu,S. (2014) Skewer: a fast and accurate adapter trimmer for next-generation sequencing paired-end reads. *BMC Bioinformatics*, **15**, 182.
61. Li,H. and Durbin,R. (2009) Fast and accurate short read alignment with burrows-wheeler transform. *Bioinformatics*, **25**, 1754–1760.
62. Li,H., Handsaker,B., Wysoker,A., Fennell,T., Ruan,J., Homer,N., Marth,G., Abecasis,G. and Durbin,R. (2009) The sequence alignment/map format and SAMtools. *Bioinformatics*, **25**, 2078–2079.
63. Zhang,Y., Liu,T., Meyer,C.A., Eeckhoute,J., Johnson,D.S., Bernstein,B.E., Nussbaum,C., Myers,R.M., Brown,M., Li,W. *et al.* (2008) Model-based analysis of chip-Seq (MACS). *Genome Biol.*, **9**, R137.
64. Ramírez,F., Ryan,D.P., Grüning,B., Bhardwaj,V., Kilpert,F., Richter,A.S., Heyne,S., Dündar,F. and Manke,T. (2016) deepTools2: a next generation web server for deep-sequencing data analysis. *Nucleic Acids Res.*, **44**, 160–165.
65. Hu,B., Petela,N., Kurze,A., Chan,K.L., Chapard,C. and Nasmyth,K. (2015) Biological chromodynamics: a general method for measuring protein occupancy across the genome by calibrating chip-seq. *Nucleic Acids Res.*, **43**, e132.
66. Martin,M. (2011) Cutadapt removes adapter sequences from high-throughput sequencing reads. *EMBnet J.*, **17**, 10–12.
67. Langmead,B. and Salzberg,S.L. (2012) Fast gapped-read alignment with bowtie 2. *Nat. Methods*, **9**, 357–359.
68. Langmead,B., Trapnell,C., Pop,M. and Salzberg,S.L. (2009) Ultrafast and memory-efficient alignment of short DNA sequences to the human genome. *Genome Biol.*, **10**, R25.
69. Kaplan,N., Moore,I.K., Fondufe-Mittendorf,Y., Gossett,A.J., Tillo,D., Field,Y., LeProust,E.M., Hughes,T.R., Lieb,J.D., Widom,J. *et al.* (2009) The DNA-encoded nucleosome organization of a eukaryotic genome. *Nature*, **458**, 362–366.
70. McKnight,J.N., Tsukiyama,T. and Bowman,G.D. (2016) Sequence-targeted nucleosome sliding in vivo by a hybrid Chd1 chromatin remodeler. *Genome Res.*, **26**, 693–704.

71. Chen,K., Xi,Y., Pan,X., Li,Z., Kaestner,K., Tyler,J., Dent,S., He,X. and Li,W. (2013) DANPOS: dynamic analysis of nucleosome position and occupancy by sequencing. *Genome Res.*, **23**, 341–351.
72. Gruber,S., Haering,C.H. and Nasmyth,K. (2003) Chromosomal cohesin forms a ring. *Cell*, **112**, 765–777.
73. Pakchuen,S., Ishibashi,M., Takakusagi,E., Shirahige,K. and Sutani,T. (2016) Physical association of *Saccharomycescerevisiae* polo-like kinase Cdc5 with chromosomal cohesin facilitates DNA damage response. *J. Biol. Chem.*, **291**, 17228–17246.
74. Alexandru,G., Uhlmann,F., Mechtler,K., Poupart,M.A. and Nasmyth,K. (2001) Phosphorylation of the cohesin subunit Scc1 by Polo/Cdc5 kinase regulates sister chromatid separation in yeast. *Cell*, **105**, 459–472.
75. Hu,B., Itoh,T., Mishra,A., Katoh,Y., Chan,K.L., Upcher,W., Godlee,C., Roig,M.B., Shirahige,K. and Nasmyth,K. (2011) ATP hydrolysis is required for relocating cohesin from sites occupied by its Scc2/4 loading complex. *Curr. Biol.*, **21**, 12–24.
76. Ivanov,D., Schleiffer,A., Eisenhaber,F., Mechtler,K., Haering,C.H. and Nasmyth,K. (2002) Eco1 is a novel acetyltransferase that can acetylate proteins involved in cohesion. *Curr. Biol.*, **12**, 323–328.
77. Onn,I., Guacci,V. and Koshland,D.E. (2009) The zinc finger of Eco1 enhances its acetyltransferase activity during sister chromatid cohesion. *Nucleic Acids Res.*, **37**, 6126–6134.
78. Rowland,B.D., Roig,M.B., Nishino,T., Kurze,A., Uluocak,P., Mishra,A., Beckouët,F., Underwood,P., Metson,J., Imre,R. *et al.* (2009) Building sister chromatid cohesion: Smc3 acetylation counteracts an antiestablishment activity. *Mol. Cell*, **33**, 763–774.
79. Kothiwal,D. and Laloraya,S. (2019) A SIR-independent role for cohesin in subtelomeric silencing and organization. *Proc. Natl. Acad. Sci. U.S.A.*, **116**, 5659–5664.
80. Maya-Miles,D., Andújar,E., Pérez-Alegre,M., Murillo-Pineda,M., Barrientos-Moreno,M., Cabello-Lobato,M.J., Gómez-Marín,E., Morillo-Huesca,M. and Prado,F. (2019) Crosstalk between chromatin structure, cohesin activity and transcription. *Epigenetics Chromatin*, **12**, 47.
81. Gullerova,M. and Proudfoot,N.J. (2008) Cohesin complex promotes transcriptional termination between convergent genes in *S. pombe*. *Cell*, **132**, 983–995.
82. Mattingly,M., Seidel,C., Muñoz,S., Hao,Y., Zhang,Y., Wen,Z., Florens,L., Uhlmann,F. and Gerton,J.L. (2022) Mediator recruits the cohesin loader Scc2 to RNA pol II-transcribed genes and promotes sister chromatid cohesion. *Curr. Biol.*, **32**, 2884–2896.
83. Muñoz,S., Jones,A., Bouchoux,C., Gilmore,T., Patel,H. and Uhlmann,F. (2022) Functional crosstalk between the cohesin loader and chromatin remodelers. *Nat. Commun.*, **13**, 7698.
84. Uusküla-Reimand,L., Hou,H., Samavarchi-Tehrani,P., Rudan,M.V., Liang,M., Medina-Rivera,A., Mohammed,H., Schmidt,D., Schwalie,P., Young,E.J. *et al.* (2016) Topoisomerase II beta interacts with cohesin and CTCF at topological domain borders. *Genome Biol.*, **17**, 182.
85. Kim,J.S., He,X., Liu,J., Duan,Z., Kim,T., Gerard,J., Kim,B., Pillai,M.M., Lane,W.S., Noble,W.S. *et al.* (2019) Systematic proteomics of endogenous human cohesin reveals an interaction with diverse splicing factors and RNA-binding proteins required for mitotic progression. *J. Biol. Chem.*, **294**, 8760–8772.
86. Kagey,M.H., Newman,J.J., Bilodeau,S., Zhan,Y., Orlando,D.A., van Berkum,N.L., Ebmeier,C.C., Goossens,J., Rahl,P.B., Levine,S.S. *et al.* (2010) Mediator and cohesin connect gene expression and chromatin architecture. *Nature*, **467**, 430–435.
87. Söderberg,O., Gullberg,M., Jarvius,M., Ridderstråle,K., Leuchowius,K.J., Jarvius,J., Wester,K., Hydbring,P., Bahram,F., Larsson,L.G. *et al.* (2006) Direct observation of individual endogenous protein complexes in situ by proximity ligation. *Nat. Methods*, **3**, 995–1000.
88. Söderberg,O., Leuchowius,K.J., Gullberg,M., Jarvius,M., Weibrecht,I., Larsson,L.G. and Landegren,U. (2008) Characterizing proteins and their interactions in cells and tissues using the in situ proximity ligation assay. *Methods*, **45**, 227–232.
89. Andersen,S.S., Hvid,M., Pedersen,F.S. and Deleuran,B. (2013) Proximity ligation assay combined with flow cytometry is a powerful tool for the detection of cytokine receptor dimerization. *Cytokine*, **64**, 54–57.
90. Leuchowius,K.J., Weibrecht,I. and Söderberg,O. (2011) In situ proximity ligation assay for microscopy and flow cytometry. *Curr. Protoc. Cytom.*, **56**, 9.36.1–9.36.15.
91. Nillegoda,N.B., Stank,A., Malinverni,D., Alberts,N., Szlachcic,A., Barducci,A., de Los Rios,P., Wade,R.C. and Bukau,B. (2017) Evolution of an intricate J-protein network driving protein disaggregation in eukaryotes. *Elife*, **6**, e24560.
92. Tsukiyama,T., Palmer,J., Landel,C.C., Shiloach,J. and Wu,C. (1999) Characterization of the imitation switch subfamily of ATP-dependent chromatin-remodeling factors in *Saccharomyces cerevisiae*. *Genes Dev.*, **13**, 686–697.
93. Varadi,M., Anyango,S., Deshpande,M., Nair,S., Natassia,C., Yordanova,G., Yuan,D., Stroe,O., Wood,G., Laydon,A. *et al.* (2022) AlphaFold protein structure database: massively expanding the structural coverage of protein-sequence space with high-accuracy models. *Nucleic Acids Res.*, **50**, D439–D444.
94. Ünal,E., Heidinger-Pauli,J.M., Kim,W., Guacci,V., Onn,I., Gygi,S.P. and Koshland,D.E. (2008) A molecular determinant for the establishment of sister chromatid cohesion. *Science*, **321**, 566–569.
95. Fernius,J. and Marston,A.L. (2009) Establishment of cohesion at the pericentromere by the Ctf19 kinetochore subcomplex and the replication fork-associated factor, Csm3. *PLoS Genet*, **5**, e1000629.
96. Li,J., Bergmann,L., Rafael de Almeida,A., Webb,K.M., Gogol,M.M., Voigt,P., Liu,Y., Liang,H. and Smolle,M.M. (2022) H3K36 methylation and DNA-binding both promote Ioc4 recruitment and Isw1b remodeler function. *Nucleic Acids Res.*, **50**, 2549–2565.
97. Lee,H.S., Lin,Z., Chae,S., Yoo,Y.S., Kim,B.G., Lee,Y., Johnson,J.L., Kim,Y.S., Cantley,L.C., Lee,C.W. *et al.* (2018) The chromatin remodeler RSF1 controls centromeric histone modifications to coordinate chromosome segregation. *Nat. Commun.*, **9**, 3848.
98. Perpelescu,M., Nozaki,N., Obuse,C., Yang,H. and Yoda,K. (2009) Active establishment of centromeric CENP-A chromatin by RSF complex. *J. Cell Biol.*, **185**, 397–407.
99. Izuta,H., Ikeno,M., Suzuki,N., Tomonaga,T., Nozaki,N., Obuse,C., Kisu,Y., Goshima,N., Nomura,F., Nomura,N. *et al.* (2006) Comprehensive analysis of the ICEN (Interphase centromere complex) components enriched in the CENP-A chromatin of human cells. *Genes to Cells*, **11**, 673–684.
100. Zentner,G.E., Tsukiyama,T. and Henikoff,S. (2013) IswI and Chd chromatin remodelers bind promoters but act in gene bodies. *PLoS Genet*, **9**, e1003317.
101. Parnell,T.J., Schlichter,A., Wilson,B.G. and Cairns,B.R. (2015) The chromatin remodelers RSC and ISW1 display functional and chromatin-based promoter antagonism. *Elife*, **4**, e06073.
102. Jain,D., Baldi,S., Zabel,A., Straub,T. and Becker,P.B. (2015) Active promoters give rise to false positive 'Phantom peaks' in ChIP-seq experiments. *Nucleic Acids Res.*, **43**, 6959–6968.
103. Wiles,E.T., Mumford,C.C., McNaught,K.J., Tanizawa,H. and Selker,E.U. (2022) The ACF chromatin remodeling complex is essential for polycomb repression. *Elife*, **11**, e77595.
104. Stanne,T., Narayanan,M.S., Ridewood,S., Ling,A., Witmer,K., Kushwaha,M., Wiesler,S., Wickstead,B., Wood,J. and Rudenko,G. (2015) Identification of the ISWI chromatin remodeling complex of the early branching eukaryote *Trypanosoma brucei*. *J. Biol. Chem.*, **290**, 26954–26967.
105. Hedouin,S., Logsdon,G.A., Underwood,J.G. and Biggins,S. (2022) A transcriptional roadblock protects yeast centromeres. *Nucleic Acids Res.*, **50**, 7801–7781.
106. Chen,C.F., Pohl,T.J., Chan,A., Slocum,J.S. and Zakian,V.A. (2019) *Saccharomyces cerevisiae* centromere RNA is negatively regulated by Cbf1 and its unscheduled synthesis impacts CenH3 binding. *Genetics*, **213**, 465–479.
107. Ling,Y.H. and Yuen,K.W.Y. (2019) Point centromere activity requires an optimal level of centromeric noncoding RNA. *Proc. Natl. Acad. Sci. USA*, **116**, 6270–6279.
108. Hemmerich,P., Stoyan,T., Wieland,G., Koch,M., Lechner,J. and Diekmann,S. (2000) Interaction of yeast kinetochore proteins with centromere-protein/transcription factor Cbf1. *Proc. Natl. Acad. Sci. U.S.A.*, **97**, 12583–12588.
109. Moreau,J.L., Lee,M., Mahachi,N., Vary,J., Mellor,J., Tsukiyama,T. and Goding,C.R. (2003) Regulated displacement of TBP from the PHO8 promoter in vivo requires Cbf1 and the Isw1 chromatin remodeling complex. *Mol. Cell*, **11**, 1609–1620.

110. Kent,N.A., Eibert,S.M. and Mellor,J. (2004) Cbf1p is required for chromatin remodeling at promoter-proximal CACGTG motifs in yeast. *J. Biol. Chem.*, **279**, 27116–27123.
111. Hinshaw,S.M., Makrantoni,V., Kerr,A., Marston,A.L. and Harrison,S.C. (2015) Structural evidence for Scc4-dependent localization of cohesin loading. *Elife*, **4**, e06057.
112. Eckert,C.A., Gravdahl,D.J. and Megee,P.C. (2007) The enhancement of pericentromeric cohesin association by conserved kinetochore components promotes high-fidelity chromosome segregation and is sensitive to microtubule-based tension. *Genes Dev.*, **21**, 278–291.
113. Davidse,L.C. (1986) Benzimidazole fungicides: mechanism of action and biological impact. *Annu. Rev. Phytopathol.*, **24**, 43–65.
114. Lee,C.K., Shibata,Y., Rao,B., Strahl,B.D. and Lieb,J.D. (2004) Evidence for nucleosome depletion at active regulatory regions genome-wide. *Nat. Genet.*, **36**, 900–905.
115. Lee,W., Tillo,D., Bray,N., Morse,R.H., Davis,R.W., Hughes,T.R. and Nislow,C. (2007) A high-resolution atlas of nucleosome occupancy in yeast. *Nat. Genet.*, **39**, 1235–1244.
116. Cole,H.A., Howard,B.H. and Clark,D.J. (2011) The centromeric nucleosome of budding yeast is perfectly positioned and covers the entire centromere. *Proc. Natl. Acad. Sci. U.S.A.*, **108**, 12687–12692.
117. Henikoff,S., Ramachandran,S., Krassovsky,K., Bryson,T.D., Codomo,C.A., Brogaard,K., Widom,J., Wang,J.-P. and Henikoff,J.G. (2014) The budding yeast centromere DNA element II wraps a stable Cse4 hemisome in either orientation in vivo. *Elife*, **3**, e01861.
118. Krassovsky,K., Henikoff,J.G. and Henikoff,S. (2012) Tripartite organization of centromeric chromatin in budding yeast. *Proc. Natl. Acad. Sci. U.S.A.*, **109**, 243–248.
119. Furuyama,S. and Biggins,S. (2007) Centromere identity is specified by a single centromeric nucleosome in budding yeast. *Proc. Natl. Acad. Sci. U.S.A.*, **104**, 14706–14711.
120. Bloom,K. and Costanzo,V. (2017) Centromere structure and function. *Prog. Mol. Subcell. Biol.*, **56**, 515–539.
121. Cheblal,A., Challa,K., Seeber,A., Shimada,K., Yoshida,H., Ferreira,H.C., Amitai,A. and Gasser,S.M. (2020) DNA damage-induced nucleosome depletion enhances homology search independently of local break movement. *Mol. Cell*, **80**, 311–326.
122. Kramarz,K. and Dziadkowiec,D. (2022) Rrp1, Rrp2 and Uls1 – yeast SWI2/SNF2 DNA dependent translocases in genome stability maintenance. *DNA Repair (Amst)*, **116**, 103356.
123. Kikuchi,S., Borek,D.M., Otwinowski,Z., Tomchick,D.R. and Yu,H. (2016) Crystal structure of the cohesin loader Scc2 and insight into cohesinopathy. *Proc. Natl. Acad. Sci. U.S.A.*, **113**, 12444–12449.
124. Xella,B., Goding,C., Agricola,E., Di Mauro,E. and Caserta,M. (2006) The ISWI and CHD1 chromatin remodelling activities influence ADH2 expression and chromatin organization. *Mol. Microbiol.*, **59**, 1531–1541.
125. Chacin,E., Reusswig,K.U., Furtmeier,J., Bansal,P., Karl,L.A., Pfander,B., Straub,T., Korber,P. and Kurat,C.F. (2023) Establishment and function of chromatin organization at replication origins. *Nature*, **616**, 836–842.
126. Petela,N.J., Llamazares,A.G., Dixon,S., Hu,B., Lee,B.G., Metson,J., Seo,H., Ferrer-Harding,A., Voulgaris,M., Gligoris,T. *et al.* (2021) Folding of cohesin's coiled coil is important for Scc2/4-induced association with chromosomes. *Elife*, **10**, e67268.
127. Horz,W. and Altenburger,W. (1981) Sequence specific cleavage of DNA by micrococcal nuclease. *Nucleic Acids Res.*, **9**, 2643–2658.
128. Dingwall,C., Lomonossoff,G.P. and Laskey,R.A. (1981) High sequence specificity of micrococcal nuclease. *Nucleic Acids Res.*, **9**, 2659–2673.
129. Clarke,E. (1998) Centromeres: proteins, protein complexes, and repeated domains at centromeres of simple eukaryotes. *Curr. Opin. Genet. Dev.*, **8**, 212–218.
130. Stigler,J., Çamdere,G., Koshland,D.E. and Greene,E.C. (2016) Single-molecule imaging reveals a collapsed conformational state for DNA-bound cohesin. *Cell Rep.*, **15**, 988–998.
131. Brownlee,P.M., Chambers,A.L., Cloney,R., Bianchi,A. and Downs,J.A. (2014) BAF180 promotes cohesion and prevents genome instability and aneuploidy. *Cell Rep.*, **6**, 973–981.
132. Hakimi,M.A., Bochar,D.A., Schmiesing,J.A., Dong,Y., Barak,O.G., Spelcher,D.W., Yokomori,K. and Shiekhattar,R. (2002) A chromatin remodelling complex that loads cohesin onto human chromosomes. *Nature*, **418**, 994–998.
133. Zikmund,T., Paszekova,H., Kokavec,J., Kerbs,P., Thakur,S., Turkova,T., Tauchmanova,P., Greif,P.A. and Stopka,T. (2020) Loss of ISWI ATPase SMARCA5 (SNF2H) in acute myeloid leukemia cells inhibits proliferation and chromatid cohesion. *Int. J. Mol. Sci.*, **21**, 2073.
134. Lovejoy,C.A., Takai,K., Huh,M.S., Picketts,D.J. and de Lange,T. (2020) ATRX affects the repair of telomeric DSBs by promoting cohesion and a DAXX-dependent activity. *PLoS Biol.*, **18**, e3000594.
135. Ritchie,K., Seah,C., Moulin,J., Isaac,C., Dick,F. and Bérubé,N.G. (2008) Loss of ATRX leads to chromosome cohesion and congression defects. *J. Cell. Biol.*, **180**, 315–324.
136. Waldman,T. (2020) Emerging themes in cohesin cancer biology. *Nat. Rev. Cancer*, **20**, 504–515.
137. van der Lelij,P., Chrzanowska,K.H., Godthelp,B.C., Rooimans,M.A., Oostra,A.B., Stumm,M., Zdzienicka,M.Z., Joenje,H. and de Winter,J.P. (2010) Warsaw breakage syndrome, a cohesinopathy associated with mutations in the XPD helicase family member DDX11/ChlR1. *Am. J. Hum. Genet.*, **86**, 262–266.
138. Antony,J., Vin Chin,C. and Horsfield,J.A. (2021) Cohesin mutations in cancer: emerging therapeutic targets. *I. J. Mol. Sci.*, **22**, 6788.
139. Liu,J. and Krantz,I.D. (2008) Cohesin and human disease. *Annu. Rev. Genomics Hum. Genet.*, **9**, 303–320.
140. Sahu,R.K., Singh,S. and Tomar,R.S. (2020) The mechanisms of action of chromatin remodelers and implications in development and disease. *Biochem. Pharmacol.*, **180**, 114200.
141. Mirabella,A.C., Foster,B.M. and Bartke,T. (2016) Chromatin deregulation in disease. *Chromosoma*, **125**, 75–93.